AD_____

Award Number: DAMD17-03-1-0251

TITLE: Rational Inhibitors of DNA Base Excision Repair (BER) Enzymes: New Tools for Elucidating the Role of BER in Cancer Chemotherapy

PRINCIPAL INVESTIGATOR: Daniel J. Krosky
James T. Stivers, Ph.D.

CONTRACTING ORGANIZATION: Johns Hopkins University
Baltimore, Maryland 21205-2196

REPORT DATE: May 2004

TYPE OF REPORT: Annual Summary

PREPARED FOR: U.S. Army Medical Research and Materiel Command
Fort Detrick, Maryland 21702-5012

REPORT DOCUMENTATION PAGE

Form Approved
OMB No. 074-0188

1. AGENCY USE ONLY (Leave blank)	2. REPORT DATE	3. REPORT TYPE AND DATES COVERED
	May 2004	Annual Summary (21 Apr 03-20 Apr 04)

4. TITLE AND SUBTITLE
Rational Inhibitors of DNA Base Excision Repair (BER) Enzymes: New Tools for Elucidating the Role of BER in Cancer Chemotherapy

5. FUNDING NUMBERS
DAMD17-03-1-0251

6. AUTHOR(S)
Daniel J. Krosky
James T. Stivers, Ph.D.

7. PERFORMING ORGANIZATION NAME(S) AND ADDRESS(ES)
Johns Hopkins University
Baltimore, Maryland 21205-2196

E-Mail: dkrosky1@jhmi.edu

8. PERFORMING ORGANIZATION REPORT NUMBER

9. SPONSORING / MONITORING AGENCY NAME(S) AND ADDRESS(ES)
U.S. Army Medical Research and Materiel Command
Fort Detrick, Maryland 21702-5012

10. SPONSORING / MONITORING AGENCY REPORT NUMBER

11. SUPPLEMENTARY NOTES

12a. DISTRIBUTION / AVAILABILITY STATEMENT
Approved for Public Release; Distribution Unlimited

12b. DISTRIBUTION CODE

13. ABSTRACT (Maximum 200 Words)

In this funding period we have completed Task 1 of the approved Statement of Work which seeks to develop useful inhibitor scaffolds for the DNA repair enzyme uracil DNA glycosylase (UDG). In addition, we have performed groundbreaking studies that shed light on the molecular basis of substrate recognition by UDG. These new studies provide exciting avenues for rational inhibitor development with potential for anticancer therapy. Major findings in this period include the synthesis and screening of new bipartite transition state-based inhibitors for UDG, and the exploration of the roles of hydrogen bonding and molecular flexibility in specific recognition by the enzyme. This work has resulted in two publications during this period.

14. SUBJECT TERMS
Uracil DNA glycosylase, inhibitors, 5-fluorouracil, breast cancer

15. NUMBER OF PAGES
32

16. PRICE CODE

17. SECURITY CLASSIFICATION OF REPORT	18. SECURITY CLASSIFICATION OF THIS PAGE	19. SECURITY CLASSIFICATION OF ABSTRACT	20. LIMITATION OF ABSTRACT
Unclassified	Unclassified	Unclassified	Unlimited

Table of Contents

Cover.....1

SF 298.....2

Table of Contents.....3

Introduction.....4

Body.....4

Key Research Accomplishments.....5

Reportable Outcomes.....5

Conclusions.....5

References.....5

Appendices.....5

INTRODUCTION

This program seeks to obtain a fundamental understanding of the chemical mechanisms by which enzymes repair damaged DNA, and to use this information to design small molecule inhibitors of these enzymes. The driving force for these efforts is the recognition that the effectiveness of cancer chemotherapy regimes is intimately connected to, and in some cases directly relies on, DNA damage repair pathways. A more sophisticated understanding of the roles of DNA damage repair in the pharmacology of DNA replication inhibitors will allow for the design of better treatments against breast and other cancers.

Studies during this period have focused primarily on Task 1 in the original Statement of Work, and this task has been essentially completed. We have also explored the question of how uracil DNA glycosylase (UDG) binds substrates with such high affinity, with the goal of using this knowledge to synthesize better rationally designed inhibitors of the enzyme. Finally, we have begun work on Task 2 by developing a new high throughput screen for UDG that will allow us to identify inhibitors from large chemical libraries. This reporting period has produced two publications in peer-reviewed journals.

BODY

As described in Specific Aim 1 of the proposal, we have now designed, synthesized and screened mechanism-based inhibitors of UDG (see Appendix, publication 1). This work, which is in press in the journal *Bioorganic Chemistry*, has uncovered two useful inhibitors that are based on the nature of the two transition-states for the reaction. We have screened a directed library of uracil analogues for those that act most potently against the enzyme, and we have gone on to tether these analogues to the 1-azadeoxyribose sugar, as described in the original proposal. The molecules that have emerged from these studies are the most potent inhibitors of UDG yet discovered (K_i values in the range 100 pM to 14 nM).

We have moved on to investigate what features of the DNA substrate are important for high affinity binding. This work, which has been published in the journal *Biochemistry* (see Appendix, publication 2), has revealed that tight binding molecules can be constructed if the uracil substrate is presented to the enzyme in the context of a base pair that lacks hydrogen bonds.

Finally, we have developed a robust high throughput assay that allows the detection of abasic sites in DNA generated by UDG (Fig. 1). This assay

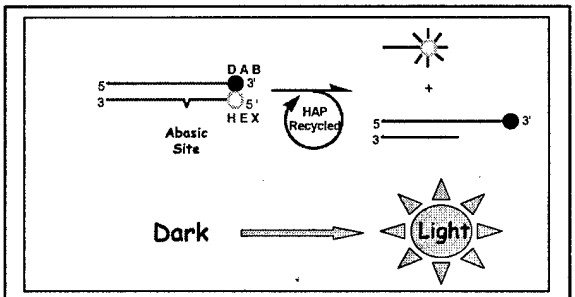

Figure 1. High throughput molecular beacon assay that detects abasic sites generated by the action of UDG. The assay relies on the action of the abasic site endonuclease (HAP), which cleaves DNA at abasic sites. The fluorescent strand (Hex) dissociates after HAP cleavage resulting in a 20-fold increase in fluorescence due to release from the quencher (DAB). The assay has been implemented in 96-well and 384-well formats

will allow rapid screening of chemical libraries as we describe in Specific Aim 2 of the proposal. This screening goal will be performed in the next funding period.

KEY RESEARCH ACCOMPLISHMENTS

- Synthesis, screening and characterization of uracil analogs that bind to the UDG-uracil pocket (SOW, Task 1).
- Performed covalent linkage of uracil analogues to the 1-azadeoyribose sugar scaffold and determined the binding affinities of the tethered molecules to UDG.
- Elucidated the molecular determinants for specific recognition of substrates by UDG (SOW, Task 1).
- Developed a novel high-throughput kinetic assay for screening inhibitors of UDG (SOW, Task 2)

REPORTABLE OUTCOMES:

This work has resulted in two published manuscripts:

1. Jiang, Y. L. Cao, C. , Stivers, J. T., Song, F. Ichikawa, Y. (2004) The Merits of Bipartite Transition-State Mimics for Inhibition of Uracil DNA Glycosylase. Bioorg Chem *In press*.

2. Krosky, D. J., Schwarz, F. P. and Stivers, J. T. (2004) Linear Free Energy Correlations for Enzymatic Base Flipping: How Do Damaged Base Pairs Facilitate Specific Recognition? Biochemistry ***43***, 4188-4195.

CONCLUSIONS:

The long-term goal of this research is to increase the effectiveness of 5-FU chemotherapy through the selective targeting of BER repair enzymes such as UDG. We have made significant progress towards this goal in this funding period through the synthesis of very potent inhibitors of the enzyme. The approaches that we have pioneered here for UDG may be generally applicable to other DNA glycosylases, and may provide general tools for targeting DNA repair pathways. The next funding period should bring significant progress towards the development of cell permeable inhibitors of UDG.

REFERENCES: None

APPENDICES: Two manuscripts are included (see above).

Available online at www.sciencedirect.com
SCIENCE DIRECT®
Bioorganic Chemistry xxx (2004) xxx–xxx
BIOORGANIC CHEMISTRY
www.elsevier.com/locate/bioorg

The merits of bipartite transition-state mimics for inhibition of uracil DNA glycosylase

Yu Lin Jiang,[a] Chunyang Cao,[a] James T. Stivers,[a,*] Fenhong Song,[b] and Yoshi Ichikawa[c]

[a] *Department of Pharmacology and Molecular Sciences, The Johns Hopkins University School of Medicine, 725 North Wolfe Street, Baltimore, MD 21205-2185, USA*
[b] *Center for Advanced Research in Biotechnology of the National Institute of Standards and Technology, University of Maryland Biotechnology Institute, Rockville, MD 20850, USA*
[c] *Optimer Pharmaceuticals, Inc., 10130 Sorrento Valley Road, Suite D, San Diego, CA 92121, USA*

Received 9 January 2004

Abstract

The glycosidic bond hydrolysis reaction of the enzyme uracil DNA glycosylase (UDG) occurs by a two-step mechanism involving complete bond breakage to the uracil anion leaving group in the first step, formation of a discrete glycosyl cation-uracil anion intermediate, followed by water attack in a second transition-state leading to the enzyme-bound products of uracil and abasic DNA. We have synthesized and determined the binding affinities of unimolecular mimics of the substrate and first transition-state (TS1) in which the uracil base is covalently attached to the sugar, and in addition, bimolecular mimics of the second addition transition state (TS2) in which the base and sugar are detached. We find that the bipartite mimics of TS2 are superior to the TS1 mimics. These results indicate that bipartite TS2 inhibitors could be useful for inhibition of glycosylases that proceed by stepwise reaction mechanisms.

Keywords: Uracil DNA glycosylase; 1-Azadeoxyribose; Transition-state mimics; Enzyme inhibition

* Corresponding author. Fax: 1-410-955-3023.
E-mail address: jstivers@jhmi.edu (J.T. Stivers).

0045-2068/$ - see front matter © 2004 Elsevier Inc. All rights reserved.
doi:10.1016/j.bioorg.2004.03.001

1. Introduction

As a DNA repair enzyme, uracil DNA glycosylase catalyzes the removal of uracil bases from DNA that may arise from the deamination of the normal base cytosine, or by misincorporation of dUTP into DNA during DNA replication [1]. Although the genome protective role of this enzyme is well-established, removal of uracil is also important or essential for the life cycle of several viruses, including pox-, herpes- and cytomegalo-, and thus inhibitors of the enzyme could serve as clinically useful antiviral agents [2–4]. In addition, inhibition of UDG could enhance the effectiveness of current anticancer therapies such as 5-fluorouracil and methotrexate that lead to increased accumulation of uracil in DNA [5,6]. Indeed, in yeast UDG knockout strains, high levels of uracil in DNA leads to cell cycle arrest at a G2 checkpoint [6], supporting the validity of this approach.

The mechanistic basis for the extraordinary catalytic power of UDG has been extensively investigated for the enzyme from *Escherichia coli* and humans [1]. A key insight from this work is that the enzyme facilitates a stepwise mechanism (Fig. 1A), that involves complete breakage of the *N*-glycosidic bond in the first transition state (TS1), the generation of a discrete oxacarbenium ion-uracil anion intermediate [7], followed by attack of the nucleophilic water at C1′ of the intermediate in the second transition state (TS2). Crystal structures have been obtained of a reactant analogue complex ($\mathbf{U}^{\Psi}$, Fig. 1B) [8], a bimolecular mimic of TS2 consisting of a cationic 1-aza-2′-deoxyribose (1-aza-dR) sugar and the uracil anion ($\mathbf{I} + \mathbf{U}^{-}$, Fig. 1B), and the reaction products of abasic DNA and uracil [9]. The cationic 1-aza-dR component of the TS2 mimic has been previously characterized as a tight binding ligand for the UDG–uracil anion binary complex ($K_D = 0.5\,nM$) [10]. The high affinity of this glycosyl cation mimic for the binary complex arises in large part from favorable electrostatic interactions with a conserved aspartate [11], the uracil anion [11], and anionic DNA phosphodiester groups [12]. In contrast, the very similar (but neutral) tetrahydrofuran abasic site product mimic binds weakly to the enzyme–uracil anion complex (Fig. 1B, $K_D > 15\,\mu M$) [10], establishing the importance of the sugar cation in promoting tight binding.

Although the previously characterized bipartite TS2 mimic is a potent inhibitor of UDG at pH values in which uracil component is anionic [10,11], at neutral pH values the affinity diminishes greatly, due to the unfavorable equilibrium for deprotonation of the base ($pK_a^{N1} = 9.8$) [11,13]. To address this shortcoming we have now synthesized monopartite mimics of TS1 in which the uracil base is covalently attached to the 1-azasugar in two ways (Fig. 1B), and we have also explored several low pK_a uracil analogues as improved coinhibitors with 1-aza-dR. We find that one of the new TS1 mimics has significantly greater affinity than two substrate analogues, and that the highest affinity TS2 mimic, consisting of 1-aza-dR and urazole ($pK_a = 5.8$), is superior at neutral pH to the original bipartite construct using uracil (Fig. 1B). The general merits and limitations of targeting TS1 and TS2 in stepwise glycosylase reactions are discussed.

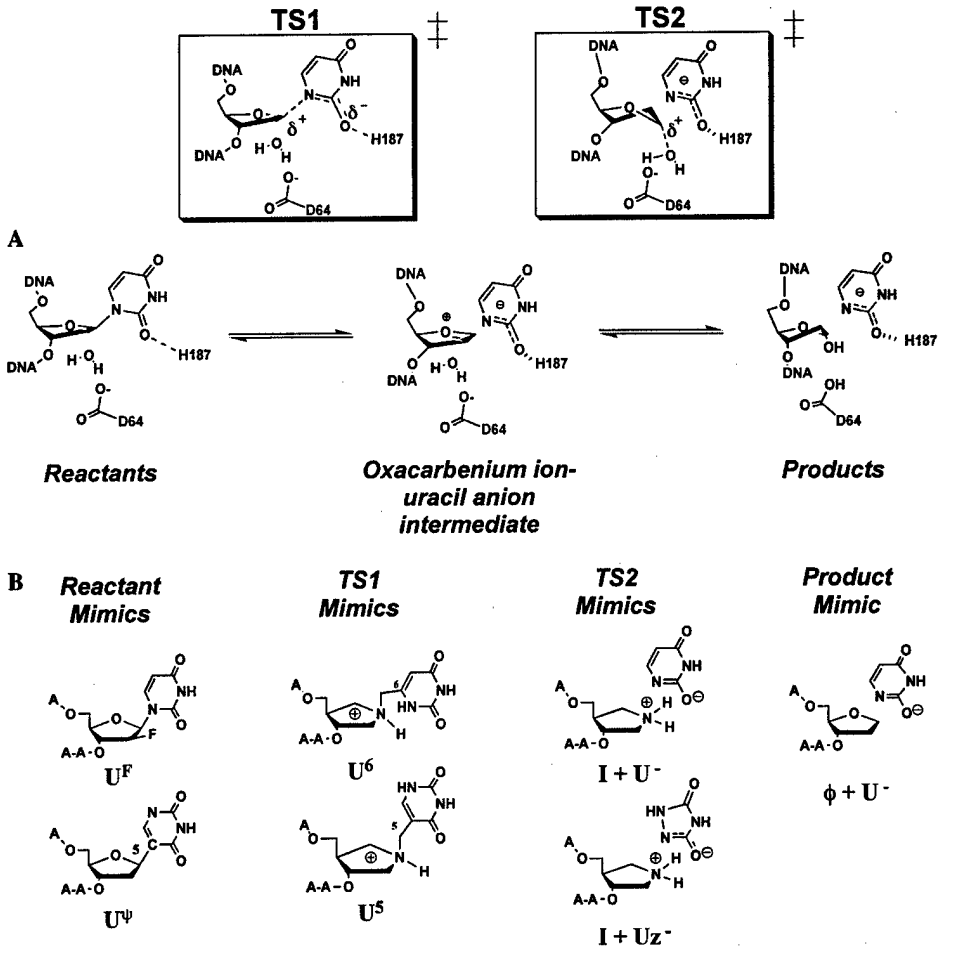

Fig. 1. The reaction coordinate of uracil DNA glycosylase (UDG) and reaction coordinate mimics. (A) UDG uses a stepwise mechanism to hydrolyze the glycosidic bond of deoxyuridine in DNA. The formation and decay of the oxacarbenium ion intermediate involves two high energy transition states (TS1 and TS2) that exhibit unique geometric and electronic features that may be mimicked by stable chemical constructs. (B) Stable chemical mimics of UDG reaction coordinate species. The 2′-fluoro-2′-deoxyuridine substrate analogue and the tetrahydrofuran abasic product analogues have been previously studied [11,15]. The other reactant and TS analogues are investigated in this work.

2. Materials and methods

2.1. Materials

As previously described, the recombinant UDG from *E. coli* strain B was purified to >99% homogeneity using a T7 polymerase-based over expression system [14]. The concentration of the enzyme was determined using an extinction coefficient of $38.5\,mM^{-1}\,cm^{-1}$.

2.2. Phosphoramidites

All nucleoside phosphoramidites were purchased from Applied Biosystems or Glen Research (Sterling, VA), except for the 2′-β-fluoro-2′-deoxyuridine phosphoramidite which was synthesized as previously described [15], and the 1-aza-1, 2-dideoxy-4α-carba-D-ribitol 5′-trityl-3′-phosphoramidite, which was synthesized as described below.

2.3. 1-Aza-1,2-dideoxy-4α-carba-D-ribitol 5′-trityl nucleoside (2)

To a solution of **1** (0.6 g, 1.67 mmol) in CH_2Cl_2 (10 ml) [16], was added NEt_3 (0.47 ml, 3.4 mmol) and Fmoc-Cl (0.52 g, 2.0 mmol). The reaction mixture was stirred under nitrogen for 2 h, and then purified by chromatography on silica with ethyl acetate–hexanes (1:1, v/v) to give product **2** (0.78 g) in 80% yeild. ^{1}H NMR ($CDCl_3$, ppm) δ 7.77 (m, 2H); 7.58 (m, 2H); 7.43 (m, 19H); 4.37 (m, 3H); 4.22 (m, 1H); 3.62 (m, 2H); 3.25 (m, 2H); 3.10 (m, 2H); and 2.42 (m, 1H).

2.4. 1-Aza-1,2-dideoxy-4α-carba-D-ribitol 5′-trityl-3′-phosphoramidite (3)

To a solution of **2** (0.226 g, 0.39 mmol) in CH_2Cl_2 (10 ml), was added diisopropylethylamine (0.2 ml) 2-cyanoethyl diisopropylchlorophosphoramidite (130 μl, 0.57 mmol). The reaction mixture was stirred under nitrogen for 0.5 h, which was purified by chromatography on silica with ethyl acetate–hexanes–NEt_3 (1:1:0.01, v/v/v) to give product **3** (0.22 g) in 71% yield. ^{1}H NMR ($CDCl_3$, ppm) δ 7.78 (m, 2H); 7.60 (m, 2H); 7.42 (m, 19H); 4.37 (m, 3H); 4.24 (m, 1H); 3.78 (m, 3H); 3.51 (m, 3H); 3.29 (m, 1H); 3.10 (m, 3H); 2.60 (m, 3H); 1.14 (m, 12H). ^{31}P NMR ($CDCl_3$, ppm) δ 150.2 (s). ESI calc for $C_{48}H_{52}N_3NaO_5P$ (M + Na) 804, found 804. This amidite is fairy unstable in trace amounts of NEt_3, which likely catalyzes the cleavage of Fmoc group, resulting in polymerization of the amidite. Therefore, the amidite should be freshly made for DNA synthesis.

2.5. Oligonucleotide synthesis

The 4 mer oligonucleotides, $\mathbf{U^F}$, $\mathbf{U^\Psi}$, **I**, and **ϕ** (see Fig. 1B), were synthesized using standard phosphoramidite chemistry with an Applied Biosystems 390 synthesizer. In these sequences, $\mathbf{U^F}$, 2′-β-fluoro-2′-deoxyuridine nucleotide; $\mathbf{U^\Psi}$, 2′-deoxypseudouridine nucleotide; **I**, 1-aza-2-dideoxy-4α-carba-D-deoxyribonucleotide; and **ϕ**, tetrahydrofuran abasic site analogue. During synthesis of oligonucleotide containing **I**, the coupling time was increased to 10 min. In addition, the time for the trityl cleavage step was increased to 180 s instead of standard 90 s. These modifications were found to increase the incorporation efficiency at this step from 30 to 80 %. After synthesis and deprotection, the oligonucleotides were purified by anion exchange HPLC and desalted by C-18 reversed phase HPLC (Phenomenex Aqua column). The correct size, purity, and nucleotide compositions of the final products were assessed by analytical reversed phase HPLC [Phenomenex Aqua column (250 mm × 10 mm)],

MALDI mass spectrometry, and by enzymatic digestion to the constituent nucleosides (see below). The concentrations of the 4 mer oligonucleotides were determined by UV absorption measurements at 260 nm, using the pair wise extinction coefficients for the constituent nucleotides [17].

2.6. Synthesis of TS1 and TS2 mimics

As outlined in Fig. 2B, the TS1 analogues with the sequences AU^{6}AA and AU^{5}AA were synthesized by derivatizing the 1-nitrogen of AIAA [12], using the appropriate uracil derivative [18].

AU^{6}AA was prepared as follows: to dry AIAA (0.9 μmol), were added H_2O (10 μl), CH_3CN (30 μl), diisopropylethylamine (10 μl), and 6-chloromethyluracil (7 μl of a 29 mg/ml solution in 90:10 MeOH/diisopropylethylamine). The clear solution was stirred for 3 days at room temperature and dried in vacuo. The final product was obtained in 50% yield from the residue by HPLC using a C-18 reverse phase column. Mass (ESI) calc for MW 1181, found 1181.

AU^{5}AA was prepared as follows: to AIAA (0.2 μmol in 20 μl H_2O), were added uracil (7 μl of a 1.1 mg/ml solution H_2O) and HCHO (9 μl of a 0.28 mg/ml solution in 48:48:4 EtOH/CH_3CN/NEt_3). The clear solution was then dried in vacuo. To this mixture, CH_3OH (5 μl) and CH_3CN (5 μl) were added. The resulting mixture was

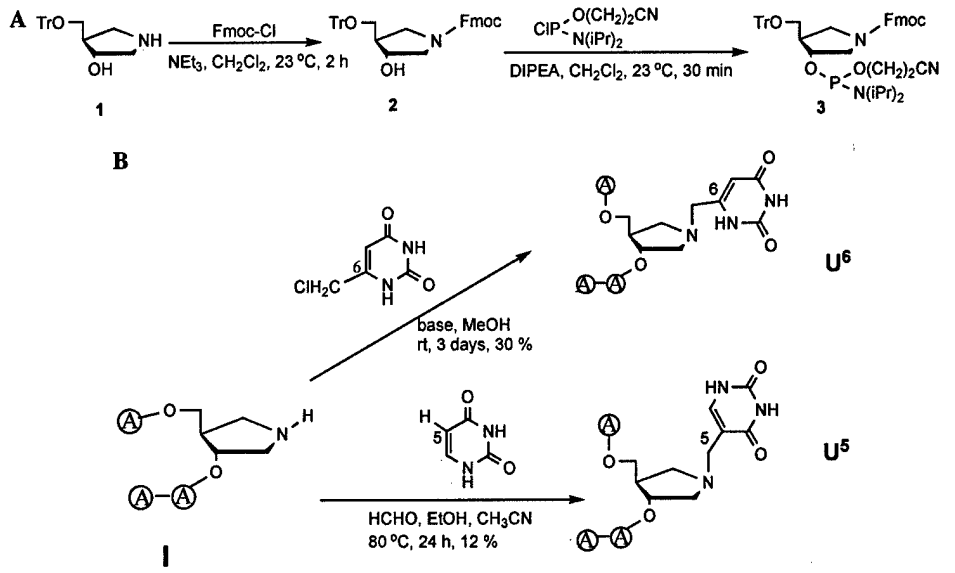

Fig. 2. Synthesis of 1-aza-deoxyribose 5′-trityl-3′-phosphoramidite (3) and the synthesis of TS1 mimics. (A) 3 was obtained through the sequential reaction of 1 with Fmoc-Cl and cyanoethyl-diisopropyl-chlorophosphoramidite. (B) 3 was incorporated into the DNA sequence A3AA (abbreviated as I throughout the text) using standard solid phase chemistry. I was used as a common synthon for the synthesis of the two TS1 analogues U^5 and U^6.

sealed and incubated at 80–85 °C for 24 h and dried in vacuo. The final product was obtained in 12% yield from the residue by HPLC using a C-18 reverse phase column. Mass (ESI) calc for MW 1181, found 1181.

2.7. Nucleotide composition analysis

The nucleotide compositions of AU^{5}AA and AU^{6}AA were confirmed by digestion with P1 nuclease and alkaline phosphatase (both obtained from Roche Diagnostics) followed by separation of the constituent nucleosides using reversed phase HPLC (Phenomenex C-18 Aqua column, 5 mm × 250 mm) with monitoring at 260 nm and isocratic elution (7% CH_3CN, 0.1 M TEAA, pH 7.0). The identity of the peaks was confirmed by comparison with the retention times of authentic nucleoside standards and the ratio of the peak areas were consistent with the expected stoichiometries and extinction coefficients of these tetramers. The standards for the 2′-deoxynucleoside forms of $\mathbf{U}^5$ and $\mathbf{U}^6$ were synthesized as previously described [18]. The structures of the deoxynucleoside standards were ascertained by ^{1}H-NMR spectroscopy and ESI–MS analyses.

2.8. Competitive inhibition measurements

For measuring the binding of the single stranded 4 mer $\mathbf{U}^F$ substrate and ϕ product analogue DNA to the free enzyme, competitive kinetic inhibition measurements were performed using the substrate ApUpAp [19]. Conditions were chosen whereby $[UDG]_{tot} \ll$ [inhibitor] or [ApUpAp], and [ApUpAp] $\ll K_m$. Accordingly, K_i could be obtained directly from a plot of k/k_0 against [inhibitor] as shown in Eq. (1), where k is the observed rate constant ($v/[UDG]_{tot}$) at a given [inhibitor], and k_0 is the observed rate constant in the absence of the inhibitor:

$$k/k_0 = 1/(1 + [X]/K_i). \quad (1)$$

For these measurements, a sensitive HPLC kinetic assay for monitoring the formation of the abasic product was employed [20]. All experiments were performed at 25 °C using TMN buffer at pH 8 (10 mM Tris–HCl, 2.5 mM $MgCl_2$, and 25 mM NaCl). For determination of the dissociation constants of the uracil analogues in Table 1, an alternative fluorescence-based competitive inhibition kinetic assay was used [10].

2.9. Binding of 1-aza-dR to the UDG binary complex

The dissociation constants for binding of **I** to the UDG–uracil or UDG–urazole complex were determined by competition binding measurements in which a 2-aminopurine (2AP) labeled abasic analogue DNA (**ϕ19**) was displaced from the EU or EUz binary complex as previously described [10]. The sequence of **ϕ19** has been previously reported [21], and this DNA construct shows a strong fluorescence decrease when it binds to the EU binary complex that can be used as a spectroscopic signal in competition binding measurements. Measurements were performed at 25 °C in TMN

buffer at pH 7 and 8. Before performing the competition binding experiments, the K_D values of **ϕ19** for the EU and EUz complexes were determined at pH 8 and 7 using direct binding measurements. In these measurements, the decrease in 2AP fluorescence was followed upon titrating a solution containing 200 nM **ϕ19** and 1 mM uracil (or urazole) with increasing concentrations of UDG. This concentration of uracil (or urazole) is over 10-fold greater than the apparent K_D of uracil or urazole for the enzyme. This insures that UDG is saturated with either base, and that the measurements reflect binding of **ϕ19** to the enzyme–base binary complex. Excitation was at 320 nm and emission spectra from 340 to 450 nm were collected using a Spex Fluoromax 3 spectrofluorimeter. The fluorescence intensity (F) at 370 nm was plotted against $[EU]_{tot}$, or $[EUz]_{tot}$ to obtain the K_D from Eq. (2), where $[X]_{tot}$ represents either $[EU]_{tot}$ or $[EUz]_{tot}$.

$$F = F_0 - \{(F_0 - F_f)[\boldsymbol{\phi 19}]_{tot}/2\}\{b - (b^2 - 4[X]_{tot}[\boldsymbol{\phi 19}]_{tot})^{1/2}\}, \quad (2)$$

$$b = K_D + [X]_{tot} + [\boldsymbol{\phi 19}]_{tot}.$$

To determine the affinity of **I** for the EU and EUz binary complexes, titrations included a saturating concentration of uracil (1 mM) so that at the beginning of the titration UDG was completely bound as E · U or E · U · **ϕ19**. The concentrations of **ϕ19** and UDG in the individual experiments are reported in the legends to Figs. 4 and 8. The dissociation constants of **I** for the EU or EUz complex ($K_D^{I,EU}$) were then determined using the computer program *Dynafit* [22] and the equilibria shown in Eqs. (3) and (4), employing the known dissociation constants of **ϕ19** for the EU and EUz complexes as determined from Eq. (2) above:

$$\mathbf{E \cdot U \cdot \phi 19} \overset{K_D^{\phi,EU}}{\rightleftharpoons} \mathbf{E \cdot U + \phi 19} \quad (3)$$

$$\mathbf{E \cdot U \cdot I} \overset{K_D^{I,EU}}{\rightleftharpoons} \mathbf{E \cdot U + I} \quad (4)$$

2.10. ^1H NMR spectroscopy

Samples (0.5 ml in 90% H_2O and 10% D_2O for frequency lock) contained 0.3 mM UDG, 2 mM uracil, 5-azauracil or urazole, 10 mM NaH_2PO_4 (pH 7.5 or 9), and 150 mM NaCl. The samples were placed in 5 mm NMR tubes (Wilmad 535-PP, Buena, NJ) and sealed with parafilm. The experiments were collected at 25 °C on a Varian INOVA 500 MHz spectrometer using a binomial 1-5-10-5-1 pulse sequence that minimizes excitation of water [23]. Acquisition and processing parameters were: 2k complex points, 68 ms acquisition time, and 15 Hz line broadening.

2.11. Computational modeling

The structural models and electrostatic potential surfaces shown in Fig. 9 were obtained with the program Spartan Pro (Wavefunction) using semi-empirical methods (HF/AM1). The truncated models included all atoms of the base and sugar, but

the 5′ and 3′ phosphodiester groups were omitted and replaced with hydrogen atoms. The reactant structure was obtained directly from the coordinates of pdb deposition 1EMH without any further optimization before calculating the electrostatic potential surface. The TS1 model was obtained by constraining the sugar in a 3′-exo conformation calculated from KIE measurements [7], and orienting the base in the position observed in the structure of uracil and 1-aza-dR (1QF3), except that the N1 nitrogen was moved to a distance of 2.75 Å from the anomeric carbon, which corresponds to a dissociative transition state with less than 0.01 bond order to the leaving group [24]. The model for TS2 was obtained directly from the structure of uracil and 1-aza-dR (1QF3) by substituting a carbon atom for the 1-NH_2^+ of the sugar. The geometry optimized structures and electrostatic potential surfaces for U^5 and U^6 in Fig. 9B were calculated using semi-empirical methods (HF/AM1), and were manually superimposed with the structural models for TS1. The model for bound urazole and 1-aza-dR in Fig. 9C was obtained from 1QF3 by substituting the appropriate atoms of the uracil base, followed by constrained energy minimization.

3. Results

3.1. Synthesis of novel TS1 analogues

The characteristics of TS1 are an elongated glycosidic bond, a significant positive charge development on the sugar, and negative charge development on the uracil leaving group (Fig. 1A). To imitate these attributes, we synthesized the two TS1 mimics shown in Fig. 1B. The first mimic (U^6), has the 1-nitrogen linked to the uracil base at the 6-position through a methylene bridge. This analogue was anticipated to imitate the elongated glycosidic bond and the developing positive charge on the sugar in a dissociative transition state. In addition, since the glycosidic nitrogen of the uracil base of U^6 is not involved in a covalent bond to the sugar, it is free to lose a proton and generate an anion in the active site, as previously observed for uracil [13,25]. This anion would be anticipated to provide stabilization to the glycosyl cation [11]. The second TS1 mimic (U^5), is similar to U^6 in that a methylene bridge connects the sugar and base (Fig. 1B). However, the bridge connects to the 5-position of the uracil, and therefore, the orientation of the base heteroatoms differs from U^6. In addition, the N1-nitrogen of U^5 is not positioned as close to the sugar as U^6, and therefore this position may not ionize and provide stabilization to the glycosyl cation.

The TS1 analogues shown in Fig. 1B were all synthesized from a common 4 mer oligonucleotide precursor (**I**) that contained the 1-azadeoxyribose moiety (Figs. 1A and B). Although UDG does bind more tightly to longer oligonucleotides [10,20], the 4 mer has been shown to possess all of the binding determinants required for tight binding of the 1-aza-dR group [10,12,19]. The 4 mer was prepared using standard solid phase phosphoramidite DNA chemistry using the commercially available adenosine nucleotide 3′-phosphoramidite, and the custom made 1-aza-1,2-dideoxy-4α-carba-D-ribitol 5′-trityl-3′-phosphoramidite (**3**, Fig. 1A) [10,16].

Once the **I** synthon was in hand (Fig. 1B), it was fairly straight forward to derivatize its 1-nitrogen with 6-chloromethyluracil or uracil in the presence of formaldehyde to yield the $\mathbf{U}^6$ and $\mathbf{U}^5$ TS1 analogues shown in Fig. 2. These syntheses are similar to those used previously to obtain analogous 1-aza-uridine nucleosides [26], but this report is the first to generate these nucleotides in a DNA scaffold. Although the yields are only in the range 12–30%, and the crude reaction products required purification by high-performance liquid chromatography, sufficient material was obtained to perform a large number of biochemical experiments.

3.2. Relative binding affinities of substrate, TS1, and bipartite TS2 analogues

Two substrate analogues, $\mathbf{U}^{\Psi}$ and $\mathbf{U}^{\mathrm{F}}$, were constructed for binding affinity comparisons with the TS1 and TS2 analogues described below (Fig. 1B). Dissociation constants for the substrate and TS1 mimics were determined by a competitive inhibition kinetic assay as previously described (Fig. 3) [12]. $\mathbf{U}^{\Psi}$ and $\mathbf{U}^{\mathrm{F}}$ were found to bind with similar affinities of 5.5 and 4.8 μM, respectively, while the TS1 mimic $\mathbf{U}^5$ bound 10 to 12-fold more tightly ($K_D = 0.5 \pm 0.04\,\mu M$). The other TS1 mimic, $\mathbf{U}^6$, was found to bind with similar affinity as the two substrate mimics ($K_D = 4.8 \pm 0.5\,\mu M$), indicating that linking uracil via a methylene bridge to the 6-position is less effective than to the 5-carbon (i.e., $\mathbf{U}^5$). These results suggest that $\mathbf{U}^5$ captures some of the electronic and geometric features of TS1.

An assumption in ascribing the enhanced binding affinity of $\mathbf{U}^5$ to mimicry of TS1 is that the 1-nitrogen of the sugar is protonated. Previous NMR and pH studies have established that the pK_a for free 1-aza-dR is 9.5, and that its nitrogen is protonated when bound to the EU^- complex in the pH range 7–9 [11]. Because direct measurement of the 1-nitrogen pK_a values in the context of $\mathbf{U}^5$ by NMR spectroscopy is not trivial, and we examined binding of $\mathbf{U}^5$ at pH 6.5 to assess whether the measurements at pH 8 involved the neutral 1-azasugar. In contrast with the anticipated increase in binding affinity if protonation of the sugar occurred as the pH was lowered from 8.0

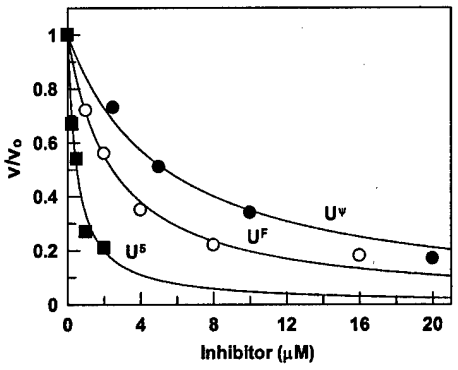

Fig. 3. Inhibition of UDG by the substrate analogues $\mathbf{U}^{\Psi}$, $\mathbf{U}^{\mathrm{F}}$, and the TS1 analogue $\mathbf{U}^5$. A competitive kinetic inhibition assay was used. The curves are nonlinear best fits to Eq. (1).

to 6.5, U^5 bound more weakly at pH 6.5, with $K_D = 8.3\,\mu M$. The weaker binding at pH 6.5 may be partially attributed to protonation of the catalytic aspartate (pK_a 6.5) that is positioned below the α face of the sugar (Fig. 1A) [9,27].

The salient features of TS2 are the lack of covalent bonding between the sugar and the anionic uracil, and significant positive charge at C1′ (Fig. 1). Thus a good mimic of TS2 is the bipartite combination of uracil and **I** (Fig. 1B). Binding of **I** to EU^- complex can be followed by competitively displacing a fluorescent abasic DNA analogue (ϕ, Fig. 4) [10], and is pH dependent because interaction of this glycosyl cation mimic is enhanced by the negative charge on the bound uracil base ($pK_a^{EU} = 7.5$) [25]. As previously shown, **I** binds very tightly at pH 8.0 with a $K_D = (5 \pm 0.4) \times 10^{-4}\,\mu M$ (solid curve, Fig. 4) [10]. However at pH 7, where the bound uracil is 75% neutral, **I** binds 300-fold more weakly ($K_D = 0.14 \pm 0.03\,\mu M$). A bar chart is shown in Fig. 5 that compares the relative affinities of the substrate and TS1 mimics at pH 8.0, and the TS2 mimic at pH 8.0 and 7.0. Although this comparison clearly reveals that the bipartite TS2 mimic ($\mathbf{I} + U^-$) is superior at pH 8.0, the Achilles' heel of this mimic is that the pK_a values for the free and bound uracil are too high to generate the required anionic form at neutral pH, leading to weak binding of both **U** and **I** under physiological conditions. A further discussion of the merits and limitations of TS2 mimicry is presented later.

3.3. Screening low pK_a uracil analogues for improved coinhibitors

One strategy to improve the potency of the TS2 mimic at a physiological pH value is to find uracil analogues that have decreased pK_a values as compared to uracil itself

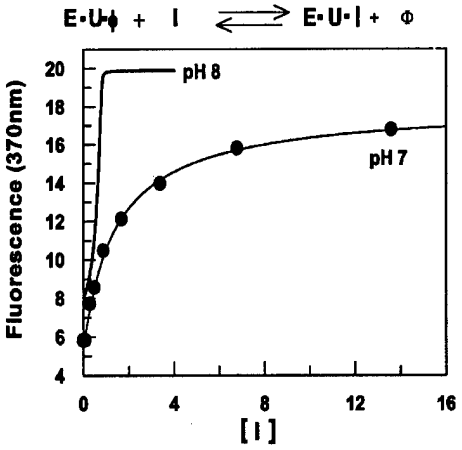

Fig. 4. pH dependence of **I** binding to the EU complex. A competitive displacement assay was used in which a fluorescent abasic site analogue (ϕ) was dissociated from the EU complex upon binding of **I** [10]. The solid curve shows the previously obtained fitted curve for binding of **I** to the EU complex at pH 8 [10]. The measurements at pH 7 used 1 mM uracil, 330 nM UDG, and 200 nM ϕ. The curve was calculated using the program *Dynafit* [22].

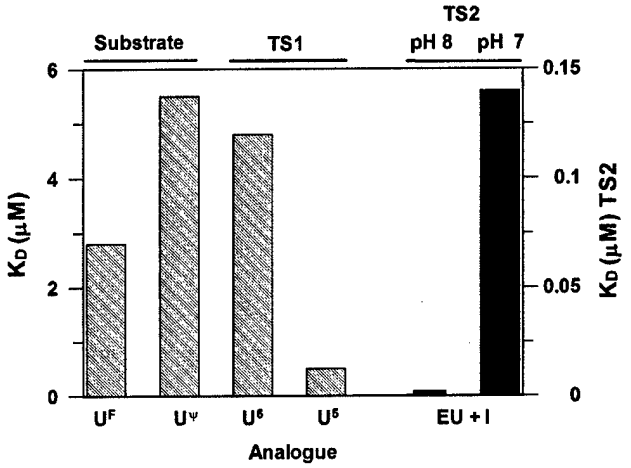

Fig. 5. Relative K_D values (μM) of substrate and TS1 analogues at pH 8.0 (left graph axis), and the bipartite TS2 mimic at pH 8.0 and 7.0 (right graph axis).

($pK_a(N1)^{free} = 9.8$, $pK_a(N1)^{bound} = 6.4$) [13]. With this aim, we screened six uracil analogues with pK_a values ranging from 5.8 to 8 for their ability to competitively inhibit the reaction of UDG at pH 8 and 7 (Table 1). As a point of reference, uracil binds 8.2-fold more weakly as the pH is lowered in this range, due to protonation of the bound uracil [25]. Most of the uracil analogues in Table 1 with $pK_a(N1)^{free}$ values of 6.7–8.0 show 1.5- to 5.9-fold weaker binding as the pH was lowered from 8 to 7, which arises from protonation of both the bound and free uracil. The magnitude of the binding decrement parallels the proton affinities of these analogues (Table 1), but it is impossible to be more quantitative about the trends because the pK_a values for the bound uracil analogues are not known. One analogue, urazole ($pK_a = 5.8$), showed pH independent binding over the pH range investigated (Fig. 6), and furthermore, bound 14-fold more tightly than uracil at pH 7 ($K_D = 98\,\mu M$) (Fig. 6B, Table 1).

Table 1
pK_a values and dissociation constants for uracil analogues[a]

	pK_a	K_d (mM)		K^8/K^{7b}
		pH 8	pH 7	
U	9.8	0.17 ± 0.02	1.4 ± 0.1	0.12
5-FU	8.0	6.2 ± 1.2	9.6 ± 1.6	0.65
6-AU	7.6	0.39 ± 0.01	1.4 ± 0.1	0.27
6-CF3-U	7.4	0.11 ± 0.01	0.30 ± 0.03	0.37
CA	7.2	0.098 ± 0.016	0.58 ± 0.11	0.17
5-AU	6.7	0.43 ± 0.04	0.98 ± 0.02	0.44
Uz	5.8	0.092 ± 0.008	0.098 ± 0.004	0.94

[a] The pK_a values for U, 5-FU, 6-AU, 6-CF_3-U, CA, 5-AU, and Uz were obtained from [46–52], respectively.

[b] The ratio of the dissociation constants at pH 8 and 7.

Because urazole showed favorable binding properties to the free enzyme, we investigated its binding interactions in more detail using NMR spectroscopy. Previous NMR studies of uracil binding to UDG have revealed the presence of a very downfield shifted proton resonance that arises from a hydrogen bond between uracil O2 and the imidazole NH of His187 in the active site (Fig. 1A) [11,13,28]. This hydrogen bond stabilizes the uracil anion in the active site by 5 kcal/mol and plays an indirect but essential role in binding of **I** by facilitating formation of the uracil anion component of the electrostatic sandwich that cradles the sugar cation [11]. To directly test whether the urazole anion persists at neutral pH in the UDG active site, we collected NMR spectra of UDG in the presence of uracil, 5-azauracil, and urazole at pH 9.0 and 7.5 (Figs. 7A and B). At pH 9.0, uracil and urazole both show the expected resonance at 14.6 and 14.8 ppm, but 5-azauracil does not. The absence of the proton resonance for 5-azauracil is consistent with its weaker binding to the enzyme, and suggests that this may be due to its improper positioning in the active site. When the pH is lowered to 7.5, only the downfield resonance of urazole remains, while that for uracil is broadened beyond the limits of detection. This NMR result strongly supports the proposal that the pH independent binding of urazole, and its enhanced af-

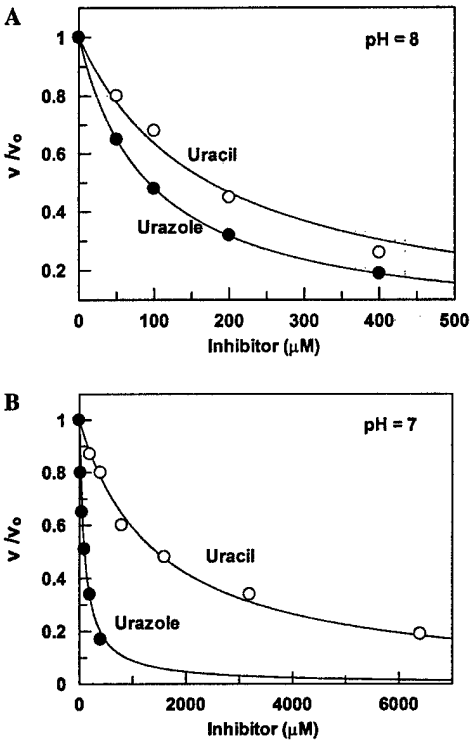

Fig. 6. Competitive inhibition of the reaction of UDG with the substrate AUAp (1 μM) by uracil and urazole at (A) pH 8 and (B) pH 7.

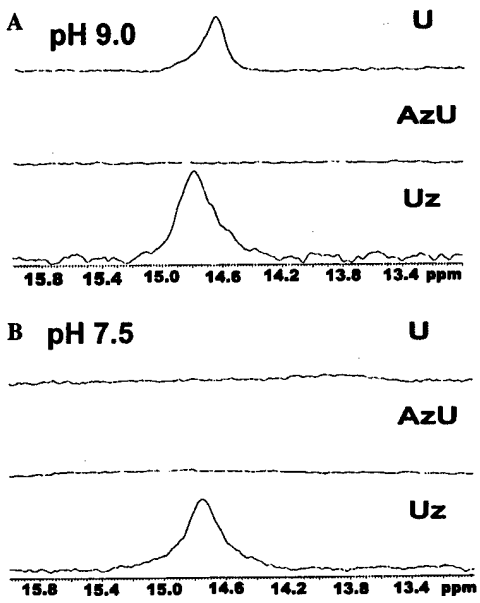

Fig. 7. ^{1}H NMR spectra of uracil (U), 5-azauracil (AzU), and urazole (Uz) bound to UDG at (A) pH 9.0 and (B) pH 7.5. The downfield resonance arises from the interaction of the $N^{\varepsilon H}$ of His187 with the O2 anion of U and Uz (see text).

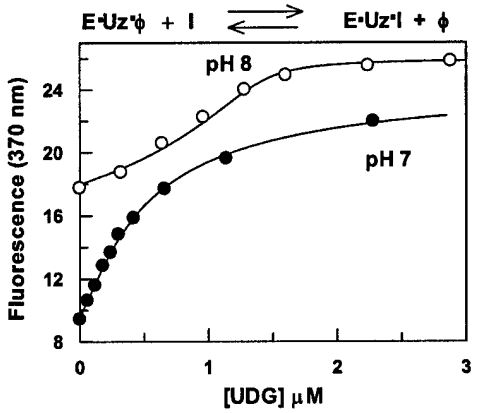

Fig. 8. Binding of I to the EUz complex at pH 8 and 7. The measurements at pH 8 used 1.4 μM UDG, 200 nM ϕ, and 1 mM urazole (Uz). The measurements at pH 7 used 330 nM UDG, 200 nM ϕ, and 1 mM urazole (Uz). The curves were calculated with the program *Dynafit* [22].

finity as compared to uracil, arises from its reduced pK_a, allowing it to be negatively charged at neutral pH.

Because of the enhanced binding of urazole at neutral pH, we investigated this analogue as a coinhibitor with I (Fig. 8). Using the competitive displacement fluorescence assay, I was found to bind to the EUz^- complex with an affinity of

14 ± 4 and 49 ± 5 nM at pH 8 and 7, respectively. Thus at a physiological pH 7.4, **I** binds to the EUz^- complex with an affinity of about 30 nM as estimated from interpolation between these measured values. This affinity is 170-fold greater than the substrate analogues bind to the free enzyme.

4. Discussion

4.1. Targeting TS1 in stepwise glycosylase reactions

Glycosylase reactions have long been amenable to the design of inhibitors that mimic features of high energy structures along the reaction coordinate, thereby capturing a portion of the enzyme's strong binding energy for these species [29–35]. In the case of a stepwise glycosylase reaction, where a discrete oxacarbenium ion intermediate is formed, it is possible to envision the design of molecules that mimic TS1, the intermediate, or TS2. In general, which of these mimics becomes the most useful inhibitor will depend on how closely the unique charge and geometric properties of these reaction coordinate species are reproduced by the inhibitor. In addition, to become useful inhibitors, bipartite intermediate and TS2 mimics must also possess sufficient binding energy to overcome the unfavorable entropic penalties associated with binding of the two molecular components from solution. A transition state mimicry strategy employing both 1′ and 4′-azasugars has been used previously to potently inhibit several DNA glycosylases [36,37].

Mimics of TS1 in which the sugar and base are covalently tethered must reproduce the elongated bond lengths of this dissociative transition state [24,38], as well as the charge distributions on the sugar and base. In addition, the linker must allow favorable positioning of the leaving group and sugar relative to enzyme groups that form stabilizing interactions with these parts of the substrate. Using the classic pseudo-thermodynamic framework developed by Radzicka and Wolfenden [39], the maximum binding affinity for a perfect TS1 mimic would be equal to $K_D = k_{non}/(k_{cat}/K_m)$, where k_{non} is the rate of the uncatalyzed glycosidic bond cleavage reaction. In the case of UDG and its substrate AUAA, $k_{non}/(k_{cat}/K_m) = 10^{-10}\ s^{-1}/(3 \times 10^6\ M^{-1}\ s^{-1}) \sim 10^{-17}$ M [1,10]. Accordingly, a perfect TS1 mimic would be expected to bind almost twelve-orders of magnitude more tightly than the U^{Ψ} and U^{F} substrate analogues (Fig. 1B). Although the TS1 mimics studied here bind as much as 12-fold more tightly than the substrate analogues, they capture only a tiny fraction of the theoretical interaction energy expected from a perfect TS1 mimic.

Previous structural and mechanistic studies provide an informative basis for understanding the comparatively weak binding affinity of the TS1 mimics. In the crystal structure of UDG bound to DNA containing the substrate analogue deoxypseudouridine (U^{Ψ}), the nucleotide base and sugar are oriented in a highly distorted conformation in which the base is nearly coplanar with the sugar ring, and the C–C glycosidic bond is elongated (1.55 Å, Fig. 9A) [8]. This ground-state conformation appears to be significantly strained, and likely represents a high energy conformation approaching that of TS1, which is highly dissociative [7]. A reasonable structural

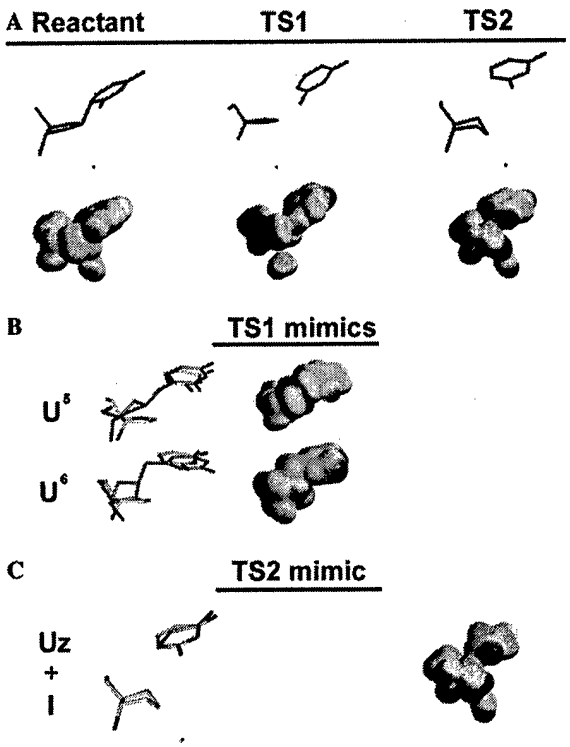

Fig. 9. Structural and electrostatic potential models for reactant, TS1, TS2, and chemical mimics. (A) Structural models for the bound substrate analogue $\mathbf{U}^{\Psi}$ and the two transition states of the stepwise reaction catalyzed by UDG. (B) Geometry optimized structural models for $\mathbf{U}^{5}$ and $\mathbf{U}^{6}$ superimposed on the model for TS1. The electrostatic potentials are plotted on the van der Waals surfaces, which are shown to the right of each model. (C) Geometry optimized structural model for the bipartite TS2 mimic of urazole and **I** superimposed on the model for TS2. The electrostatic potential surface of **Uz** + **I** is shown to the right. The details of how these models were calculated are described in Section 2.

model for TS1 is shown in Fig. 9A, which was obtained from three pieces of information (see Section 2): (i) the crystallographic coordinates of $\mathbf{U}^{\Psi}$ [8], (ii) the results from KIE studies that provide the sugar pucker and C1′–N1 bond order in TS1 (<0.01) [7], and the position of the uracil base in the crystal structure of the bipartite TS2 mimic of uracil and 1-aza-dR [40]. A model of TS1 obtained using this information is superimposed with energy minimized models of $\mathbf{U}^{6}$ and $\mathbf{U}^{5}$ in Fig. 9B. As compared to the glycosidic bond of the substrate analogue $\mathbf{U}^{\Psi}$, the methylene bridges of $\mathbf{U}^{6}$ and $\mathbf{U}^{5}$ increase the linear distance between the base and sugar from 1.55 to about 2.6 Å. However as shown in Fig. 9B, the constraints imposed by the methylene bridge groups do not allow an orientation of the base and sugar that precisely mimics that of TS1.

In addition to the relatively poor structural mimicry by $\mathbf{U}^{6}$ and $\mathbf{U}^{5}$, these analogues also poorly match the charge distribution on the sugar and base in TS1. This can be appreciated from comparison of the electrostatic potential surfaces of

these TS1 mimics with that of the TS1 model (Figs. 9A and B). For instance, $\mathbf{U}^5$ and $\mathbf{U}^6$ both mimic the positive charge character at C1′, but they poorly match the negative potential on the uracil leaving group, because the electrons of their intact glycosidic bonds are not able to delocalize onto the O2 atom of the base. A potent purine based TS1 inhibitor (**4**) analogous to $\mathbf{U}^5$ and $\mathbf{U}^6$ has been synthesized for the enzyme purine nucleoside phosphorylase (PNP) from bovine and *Mycobacterium tuberculosis* (Mt) [34,41].

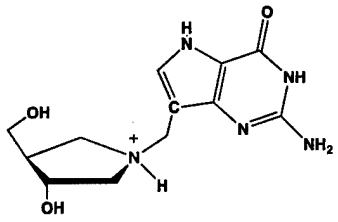

4

The MtPNP follows a dissociative but concerted mechanism and the methylene bridge analogue (**4**) presumably mimics the features of this transition-state ($K_D = 24\,pM$) [34]. In contrast, the bovine PNP shows an earlier more associative transition-state, and accordingly, (**4**) bound much more weakly [34,42]. For UDG, neither type of TS1 inhibitor is very effective because of the highly unusual orientation of the sugar and base, and the optimization of the active site towards stabilization of the electronic features of the oxacarbenium ion intermediate and TS2.

4.2. The merits of targeting TS2

The properties of TS2 are a fully dissociated uracil base, which has accumulated a full negative charge, and a glycosyl cation that will have developed some bonding to the incoming water nucleophile. The recent crystal structure of **I** and the uracil anion bound to human UDG shows that **I** assumes a distorted conformation in which the imino nitrogen is displaced from the plane of the sugar ring towards the attacking water [40]. An implication of this structure is that the planar conformation of the oxacarbenium ion intermediate is broken in TS2, and that the electrophilic anomeric carbon migrates to meet the water nucleophile. Thus, although **I** was originally thought to mimic the planar oxacarbenium ion intermediate, its nonplanar conformation, and its charge localization on the 1′ position, makes it a much better mimic of TS2. The structure and corresponding electrostatic model of the bipartite TS2 mimic consisting of urazole and **I** is shown in Fig. 9 for comparison with a model of TS2 (Fig. 9A), which was constructed from the crystallographic coordinates of 1Q3F. The excellent geometric and electrostatic match between the bipartite inhibitor and TS2 is much better than that observed for any of the TS1 mimics (see above).

The development of bipartite TS2 inhibitors for glycosylase reactions is a nontraditional approach, because a single substrate molecule is deconstructed into two

parts, each of which mimics the presumed features of a bimolecular transition state. This contrasts with the bisubstrate analogue strategy, where two reactants are covalently tethered to capture the binding energy of the two halves, thereby bypassing the entropic penalty for binding two molecules from solution [43,44]. The inherent difficulty with this bimolecular approach is that the binding of each component is comparatively weak in the absence of the other component. Thus in general, the individual binding energy of at least one of the parts must be sufficiently large to significantly populate the enzyme under physiological conditions. Under such conditions, binding of the first component creates the binding environment that allows tight binding of the second component, and creation of the high affinity bimolecular inhibitor complex. In practical terms, this requires that the intracellular concentration of at least one of the component parts be high relative to its K_D. Of course, a monopartite TS2 mimic could provide a significant entropic advantage over the bipartite mimic if the correct structural features could be captured.

In principle, the above thermodynamic problem for a bipartite inhibitor may be overcome if one of the components is also the last reaction product to be released (such as the uracil anion in this case) [10]. For such an ordered product release mechanism, the second component (1-aza-dR in this case) will bind avidly to the enzyme–product complex, and the inhibition mechanism will be noncompetitive with respect to substrate. For UDG, in vitro studies at pH 8.0 have shown that 80 nM **I** provided 95% inhibition of UDG in the absence of any added uracil coinhibitor, and that this strong inhibition arose from **I** binding tightly to the EU product complex [10]. Of course, both U and **I** also bind to the free enzyme, but these inhibition pathways will not be significant given the weak affinities of the individual parts for the free enzyme at physiological pH. A noncompetitive mode of inhibition is especially advantageous for targeting a DNA repair enzyme that not only binds to damaged target sites in DNA, but also binds nonspecifically to nontarget DNA, which is present at high concentrations in cells.

5. Conclusion

We have explored chemical analogues that mimic the features of several species along the stepwise enzymatic reaction coordinate of UDG. In general, these findings show that bipartite TS2 mimics can serve as effective inhibitors for glycosylase reactions that proceed by stepwise mechanisms. In favorable cases, the bipartite approach can offer advantages over unimolecular TS1 inhibitors because stable chemical analogues of TS2 may be better able to match the geometries and charge distributions of the cationic sugar and leaving group. Furthermore, we suggest that this strategy is likely to be most successful when the following conditions are met: (i) when one of the inhibitor components is the anionic product leaving group of the reaction, (ii) when the free and bound forms of the leaving group product have the correct anionic ionization state at physiological pH, and (iii) when the intracellular concentration of the leaving group product is comparable to or greater than its K_D. In addition, the inhibition is noncompetitive with respect to substrate, which is

desirable when high concentrations of substrate are present in the cellular environment. Several reactions that potentially meet these criteria are those catalyzed by sugar-NDP hydrolases or transferases [32,45], nucleoside phosphorylases [42], and phosphoribosyl transferases [42].

Acknowledgments

This work was supported by National Institutes of Health Grant GM46835 (J.T.S.).

References

[1] J.T. Stivers, Y.L. Jiang, Chem. Rev. 103 (2003) 2729–2759.
[2] R. Chen, H. Wang, L.M. Mansky, J. Gen. Virol. 83 (2002) 2339–2345.
[3] A.K. Millns, M.S. Carpenter, A.M. DeLange, Virology 198 (1994) 504–513.
[4] R.B. Pyles, R.L. Thompson, J. Virol. 68 (1994) 4963–4972.
[5] R.D. Ladner, Curr. Protein Pept. Sci. 2 (2001) 361–370.
[6] B.A. Tinkelenberg, M.J. Hansbury, R.D. Ladner, Cancer Res. 62 (2002) 4909–4915.
[7] R.M. Werner, J.T. Stivers, Biochemistry 39 (2000) 14054–14064.
[8] S.S. Parikh, G. Walcher, G.D. Jones, G. Slupphaug, H.E. Krokan, G.M. Blackburn, J.A. Tainer, Proc. Natl. Acad. Sci. USA 97 (2000) 5083–5088.
[9] S.S. Parikh, C.D. Mol, G. Slupphaug, S. Bharati, H.E. Krokan, J.A. Tainer, EMBO J. 17 (1998) 5214–5226.
[10] Y.L. Jiang, Y. Ichikawa, J.T. Stivers, Biochemistry 41 (2002) 7116–7124.
[11] Y.L. Jiang, A.C. Drohat, Y. Ichikawa, J.T. Stivers, J. Biol. Chem. 277 (2002) 15385–15392.
[12] Y.L. Jiang, Y. Ichikawa, F. Song, J.T. Stivers, Biochemistry 42 (2003) 1922–1929.
[13] A.C. Drohat, J.T. Stivers, J. Am. Chem. Soc. (2000) 1840–1841.
[14] A.C. Drohat, G. Xiao, M. Tordova, J. Jagadeesh, K.W. Pankiewicz, K.A. Watanabe, G.L. Gilliland, J.T. Stivers, Biochemistry 38 (1999) 11876–11886.
[15] J.T. Stivers, K.W. Pankiewicz, K.A. Watanabe, Biochemistry 38 (1999) 952–963.
[16] K. Makino, Y. Ichikawa, Tetrahedron Lett. 39 (1998) 8245–8248.
[17] G.D. Fasman, Handbook of Biochemistry and Molecular Biology: Nucleic Acids, third ed., vol. 1, CRC Press, Boca Raton, FL, 1975.
[18] V.V. Filichev, E.B. Pedersen, Tetrahedron 57 (2001) 9163–9168.
[19] Y.L. Jiang, J.T. Stivers, Biochemistry 40 (2001) 7710–7719.
[20] Y.L. Jiang, K. Kwon, J.T. Stivers, J. Biol. Chem. 276 (2001) 42347–42354.
[21] J.T. Stivers, Nucleic Acids Res. 26 (1998) 3837–3844.
[22] P. Kuzmic, Anal. Biochem. 237 (1996) 260–273.
[23] P.J. Hore, J. Magn. Reson. 61 (1983) 567–570.
[24] V.L. Schramm, Curr. Opin. Chem. Biol. 5 (2001) 556–564.
[25] A.C. Drohat, J.T. Stivers, Biochemistry 39 (2000) 11865–11875.
[26] S.U. Hansen, M. Bols, Acta Chem. Scand. 52 (1998) 1214–1222.
[27] A.C. Drohat, J. Jagadeesh, E. Ferguson, J.T. Stivers, Biochemistry 38 (1999) 11866–11875.
[28] J. Dong, A.C. Drohat, J.T. Stivers, K.W. Pankiewicz, P.R. Carey, Biochemistry 39 (2000).
[29] A. Bulow, I.W. Plesner, M. Bols, Biochim. Biophys. Acta 1545 (2001) 207–215.
[30] H. Liu, X. Liang, H. Sohoel, A. Bulow, M. Bols, J. Am. Chem. Soc. 123 (2001) 5116–5117.
[31] B.L. Mark, D.J. Vocadlo, D. Zhao, S. Knapp, S.G. Withers, M.N. James, J. Biol. Chem. 276 (2001) 42131–42137.
[32] L. Qiao, B.W. Murray, M. Shimazaki, J. Schultz, C.-H. Wong, J. Am. Chem. Soc. 118 (1996) 7653–7662.

[33] G.A. Kicska, L. Long, H. Horig, C. Fairchild, P.C. Tyler, R.H. Furneaux, V.L. Schramm, H.L. Kaufman, Proc. Natl. Acad. Sci. USA 98 (2001) 4593–4598.
[34] A. Lewandowicz, W. Shi, G.B. Evans, P.C. Tyler, R.H. Furneaux, L.A. Basso, D.S. Santos, S.C. Almo, V.L. Schramm, Biochemistry 42 (2003) 6057–6066.
[35] A. Lewandowicz, P.C. Tyler, G.B. Evans, R.H. Furneaux, V.L. Schramm, J. Biol. Chem., 2003.
[36] L. Deng, O.D. Schaerer, G.L. Verdine, J. Am. Chem. Soc. 119 (1997) 7865–7866.
[37] O.D. Scharer, H.M. Nash, J. Jiricny, J. Laval, G.L. Verdine, J. Biol. Chem. 273 (1998) 8592–8597.
[38] V.L. Schramm, W. Shi, Curr. Opin. Struct. Biol. 11 (2001) 657–665.
[39] A. Radzicka, R. Wolfenden, Science 267 (1995) 90–93.
[40] M.A. Bianchet, L.A. Seiple, Y.L. Jiang, Y. Ichikawa, L.M. Amzel, J.T. Stivers, Biochemistry 42 (2003) 12455–12460.
[41] L.A. Basso, D.S. Santos, W. Shi, R.H. Furneaux, P.C. Tyler, V.L. Schramm, J.S. Blanchard, Biochemistry 40 (2001) 8196–8203.
[42] A. Fedorov, W. Shi, G. Kicska, E. Fedorov, P.C. Tyler, R.H. Furneaux, J.C. Hanson, G.J. Gainsford, J.Z. Larese, V.L. Schramm, S.C. Almo, Biochemistry 40 (2001) 853–860.
[43] W.P. Jencks, Adv. Enzymol. Relat. Areas Mol. Biol. 43 (1975) 219–410.
[44] M.I. Page, W.P. Jencks, Proc. Natl. Acad. Sci. USA 68 (1971) 1678–1683.
[45] P.M. Legler, M.A. Massiah, A.S. Mildvan, Biochemistry 41 (2002) 10834–10848.
[46] E. Kimura, H. Kitamura, T. Koike, M. Shiro, J. Am. Chem. Soc. 119 (1997) 10909–10919.
[47] C. Thibaudeau, J. Plavec, J. Chattopadhyaya, J. Org. Chem. 61 (1996) 266–286.
[48] N.D. Goldberg, J.L. Dahl, R.E. Parks Jr., J. Biol. Chem. 238 (1963) 3109–3114.
[49] C. Heidelberger, D. Parsons, D.C. Remy, J. Am. Chem. Soc. 84 (1962) 3697–3698.
[50] R.C. Hirt, R.G. Schmitt, H.L. Strauss, J.G. Koren, J. Chem. Eng. Data 6 (1961) 610–612.
[51] A. Piskala, J. Gut, Coll. Czechoslovak Chem. Commun. 26 (1961) 2519–2529.
[52] M.J. Bausch, B. David, P. Dobrowolski, C. Guadalupe-Fasano, R. Gostowski, D. Selmarten, V. Prasad, A. Vaughn, L.H. Wang, J. Org. Chem. 56 (1991) 5643–5651.

Biochemistry **2004,** *43,* 4188−4195

APPENDIX 2

Linear Free Energy Correlations for Enzymatic Base Flipping: How Do Damaged Base Pairs Facilitate Specific Recognition?†

Daniel J. Krosky,‡ Frederick P. Schwarz,§ and James T. Stivers*,‡

Department of Pharmacology and Molecular Sciences, The Johns Hopkins School of Medicine, 725 North Wolfe Street, Baltimore, Maryland 21205, and The Center for Advanced Research in Biotechnology and National Institute of Standards and Technology, 9600 Gudelsky Drive, Rockville, Maryland 20850

Received December 22, 2003; Revised Manuscript Received February 6, 2004

ABSTRACT: To efficiently maintain their genomic integrity, DNA repair glycosylases must exhibit high catalytic specificity for their cognate damaged bases using an extrahelical recognition mechanism. One possible contribution to specificity is the weak base pairing and inherent instability of damaged sites which may lead to increased extrahelicity of the damaged base and enhanced recognition of these sites. This model predicts that the binding affinity of the enzyme should increase as the thermodynamic stability of the lesion base pair decreases, because less work is required to extrude the base into its active site. We have tested this hypothesis with uracil DNA glycosylase (UDG) by constructing a series of DNA duplexes containing a single uracil (U) opposite a variety of bases (X) that formed from zero to three hydrogen bonds with U. Linear free energy (LFE) relationships were observed that correlated UDG binding affinity with the entropy and enthalpy of duplex melting, and the dynamic accessibility of the damaged site to chemical oxidation. These LFEs indicate that the increased conformational freedom of the damaged site brought about by enthalpic destabilization of the base pair promotes the formation of extrahelical states that enhance specific recognition by as much as 3000-fold. However, given the small stability differences between normal base pairs and U·A or U·G base pairs, relative base pair stability contributes little to the $>10^6$-fold discrimination of UDG for uracil sites in cellular DNA. In contrast, the intrinsic instability of other more egregious DNA lesions may contribute significantly to the specificity of other DNA repair enzymes that bind to extrahelical bases.

The genetic information of a cell can be irreversibly altered through the chemical modification of nucleotide bases (*1*). To combat these mutagenic effects, organisms have evolved a two-tiered base excision repair (BER) pathway that handles a wide array of base lesions (*2*). In the first stage, a highly specific DNA repair glycosylase excises the damaged base from the DNA (*3*, *4*), producing an abasic site. This intermediate is then processed by the sequential action of several repair enzymes that ultimately restore the site to its original state (*2*). Since damaged site specificity resides solely with the DNA glycosylase, these enzymes must possess extraordinarily high catalytic specificities (*4*, *5*). In the absence of such specificity, undamaged bases would be randomly excised from DNA, leading to undesirable abasic sites and genetic instability (*6*−*10*).

In general, enzymatic specificity results from the extraordinary structure of enzyme active sites that disfavors formation of catalytically productive interactions with nonsubstrate molecules, and strongly favors such interactions with the true substrates. As an essential part of their recognition mechanisms, all DNA glycosylases extrude their damaged bases from the DNA double helix in a process known as base flipping, thereby placing it extrahelically into their active sites where specific interactions with the damaged base can be formed (*11*, *12*). As part of the energetic cost of base flipping, the hydrogen bonds and stacking interactions of the base pair must be disrupted. Thus, a prediction is that DNA glycosylases should bind more tightly to damaged sites with disrupted base pairing because it requires less binding energy to flip the damaged base from the destabilized site (*4*, *13*−*22*). Such a thermodynamic mechanism is quite general, and would apply even for DNA glycosylases that interact with the base that opposes the damaged base (*23*−*25*).

How much does the intrinsic thermodynamic stability of the damaged base pair contribute to specific damaged site binding by DNA glycosylases? We have investigated this question using the enzyme uracil DNA glycosylase (UDG),[1] which removes uracil from U·G and U·A base pairs in duplex DNA (*14*, *26*, *27*). The approach was to measure the binding affinity of UDG for a series of DNA duplexes, in which the number of hydrogen bonds (n) between uracil and its opposing base (X) were systematically varied (Figure 1A).

† This work was supported by NIH Grant GM56834 to J.T.S.

* To whom correspondence should be addressed: Department of Pharmacology and Molecular Sciences, Johns Hopkins School of Medicine, 725 N. Wolfe St., Baltimore, MD 21205. E-mail: jstivers@jhmi.edu.

‡ The Johns Hopkins School of Medicine.

§ The Center for Advanced Research in Biotechnology and National Institute of Standards and Technology.

[1] Abbreviations: UDG, uracil DNA glycosylase; U^F, 2′-β-fluoro-2′-deoxyuridine; ϕ, abasic site; D, 2,6-diaminopurine; M, 4-methylindole; N, nebularine; DSC, differential scanning calorimetry; ψ, pseudodihedral angle.

10.1021/bi036303y CCC: $27.50
Published on Web 03/11/2004

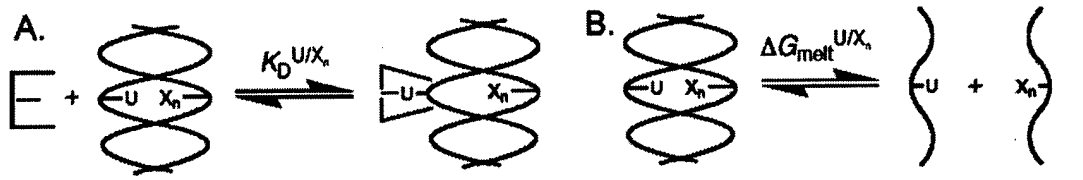

FIGURE 1: (A) Specific binding of UDG (E) to a DNA duplex containing deoxyuridine (U) opposite a purine analogue (X). In this study, the number of hydrogen bonds (n) in the U·X_n base pair varies from zero to three. Since binding of uracil requires breaking of the base pair hydrogen bonds, the difference in binding free energy ($\Delta\Delta G_{bind}$) between a DNA duplex with n hydrogen bonds and a reference duplex with three hydrogen bonds (U·X_3) should in part reflect the reduced energetic cost of breaking the hydrogen bonds in the base pair. (B) Dissociation of a duplex with a U·X_n base pair into two single strands. The difference in the duplex melting free energy ($\Delta\Delta G_{melt}$) between a U·X_n duplex and the reference duplex (U·X_3) will also reflect the energetic effects of a destabilized base pair.

Then, these binding affinities were correlated with rigorous measurements of the thermodynamic stabilities of these duplexes (Figure 1B). UDG was selected for this study because, unlike many DNA glycosylases (*23*−*25*), it does not make any direct contacts with the base opposite uracil (*11*). Thus, the observed changes in binding affinity can be largely attributed to the relative stability of the U·X_n base pairs in the free duplex DNA and not differential interactions of the enzyme with the various opposing bases. These quantitative free energy correlations provide the first direct evidence that promotion of extrahelical conformations by enthalpic destabilization of a damaged site can indeed enhance the specific binding of a DNA repair enzyme.

EXPERIMENTAL PROCEDURES[2]

Materials. The 2′-deoxynucleoside phosphoramidites, CPG supports, and DNA synthesis reagents were purchased from Glen Research (Sterling, VA), except for 2′-β-fluoro-2′-deoxyuridine (U^F), which was synthesized as described previously (*5*, *28*). The oligonucleotides were synthesized using standard phosphoramidite chemistry on an Applied Biosystems 392 synthesizer. The oligonucleotides were purified by anion exchange HPLC (Zorbax), followed by C-18 reversed phase HPLC (Phenomenex Aqua column). Fractions containing pure oligonucleotide were concentrated to dryness *in vacuo*, redissolved in MilliQ water, and stored at −20 °C. The purity of the oligonucleotides was assessed by matrix-assisted laser desorption mass spectroscopy and denaturing polyacrylamide gel electrophoresis. The concentration of each oligonucleotide was determined using its extinction coefficient at 260 nm (*29*). DNA duplexes were hybridized in 10 mM Tris-HCl (pH 8.0) and 25 mM NaCl as described previously (*5*). The purification of *Escherichia coli* UDG has been described previously (*30*).

K_D Measurements. The K_D values for binding of the U^F·X_n duplexes to UDG were measured essentially as described using a kinetic competitive inhibition HPLC assay under conditions where the apparent K_i is equal to the K_D value (i.e., [S] ≪ K_m, where S exhibits rapid equilibrium binding) (*31*). The only modification was that the abasic product (AΦAp) and reactant (AUAp) were separated using isocratic conditions with 9.5% CH_3CN and 0.1 M triethylammonium acetate. Reaction mixtures (35 μL) containing 10 mM Tris-HCl (pH 8.0), 60 mM NaCl, 12.5 μg/mL BSA, 1 μM AUAp, 0.5 nM UDG, and a variable amount of the U^F·X_n duplex were incubated at room temperature for 5 min. The K_D for each duplex was determined by fitting to eq 1

$$k_i/k_o = 1/(1 + [U^F{\cdot}X_n]/K_D) \quad (1)$$

where k_i is the inhibited rate and k_o is the rate in the absence of competitor DNA. For the tightest binding duplex (U^F·M), eq 1 was modified to take into account inhibitor depletion (*32*).

The differences in binding free energies relative to the duplex with three hydrogen bonds (U^F·D) were calculated from the measured K_D values using eq 2.

$$\Delta\Delta G_{bind} = RT \ln[K_D(U^F{\cdot}X_n)/K_D(U^F{\cdot}D)] \quad (2)$$

Fluorescence Spectroscopy. To ascertain that all of the DNA duplexes attained the same bound state, tryptophan fluorescence measurements of free and DNA-bound UDG were performed. Samples (497 μL) containing 10 mM Tris-HCl (pH 8.0), 60 mM NaCl, and 300 nM UDG were incubated for 3 min at 25 °C in a 10 mm quartz cuvette, and a fluorescence emission spectrum was recorded in the range of 325−425 nm on a SPEX FluoroMax-3 fluorimeter (λ_{ex} = 295 nm). U^F·X_n duplex DNA (2.5 μL) was then added to the UDG solution to give a final DNA concentration of 500 nM. The reaction mixture was magnetically stirred and incubated for 3 min at 25 °C, before the fluorescence emission spectrum of the UDG·DNA complex was recorded. The tryptophan fluorescence intensities of free and DNA-bound UDG at 333 nm were measured, and the raw values were then normalized for the fraction of UDG bound to each DNA analogue before the ratio ($F^{333}_{bound}/F^{333}_{free}$) was calculated.

Differential Scanning Calorimetry. DSC measurements of duplex strand melting were taken using a VP-DSC microcalorimeter from Microcal, Inc. (Northampton, MA) essentially as described previously (*33*). The DNA solutions had a concentration of 20 μM in DNA duplex with 10 mM Na_2HPO_4 (pH 7.5) and 60 mM NaCl. Samples were equilibrated at 20 °C for 15 min and scanned up to 95 °C at a preset scan rate of 60 °C/h. The transition peak areas were measured using the EXAM software program (*34*), and the transition peak areas were divided by the DNA duplex concentration to provide the transition enthalpies. Transition

[2] Certain commercial materials, instruments, and equipment are identified herein to specify the experimental procedure as completely as possible. In no case does such identification imply a recommendation or endorsement by the National Institute of Standards and Technology, nor does it imply that the material, instruments, or equipment identified is necessarily the best available for the purpose.

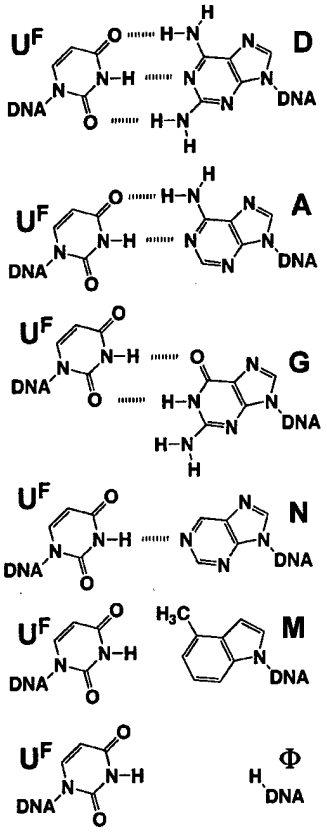

FIGURE 2: Structures of $U^F \cdot X_n$ base pairs: $U^F \cdot D$ (*54*, *55*), $U^F \cdot G$ (*56*), $U^F \cdot N$ (*57*, *58*), $U^F \cdot \Phi$ (*59*–*61*), and $U^F \cdot M$ (*62*).

entropies were determined from plots of C_p/T against T, by dividing the transition peak area by the DNA duplex concentration. Procedures for buffer baseline corrections and accounting for pre- and post-transition baselines have been described previously (*33*).

$KMnO_4$ Oxidation Measurements. Because of the low reactivity of U^F to oxidation (*35*), it was replaced with thymine (T) in the oligonucleotides used in this study. To reaction mixtures (20 μL) containing 10 mM Tris-HCl (pH 8.0), 60 mM NaCl, and either 100 nM single-stranded 5′-[^{32}P]T or 5′-[^{32}P]T·X_n duplex was added 2.5 mM $KMnO_4$. After the sample had been incubated for 3 min at room temperature, the reaction was halted by the addition of 20 μL of a stop solution containing 1.5 M sodium acetate, 1 M 2-mercaptoethanol, and 200 μg/mL tRNA. The samples were processed, imaged, and quantified as described previously (*32*).

RESULTS

Binding of UDG to Destabilized Damaged Sites. A series of 15mer duplexes were constructed in which 2′-β-fluoro-2′-deoxyuridine (U^F), a nonhydrolyzable uracil analogue (*5*), was placed opposite a series of bases (X) which form zero to three hydrogen bonds with U^F (Figure 2). The affinity of UDG for each $U^F \cdot X$ duplex was measured by a competitive inhibition kinetic assay in which a 3mer substrate (AUAp) is separated from the abasic product (AΦAp) using reverse phase HPLC (Figure 3A) (*31*). Representative inhibition data are shown in Figure 3B for the duplex that contains a uracil·4-methylindole base pair ($U^F \cdot M$). The K_D values for

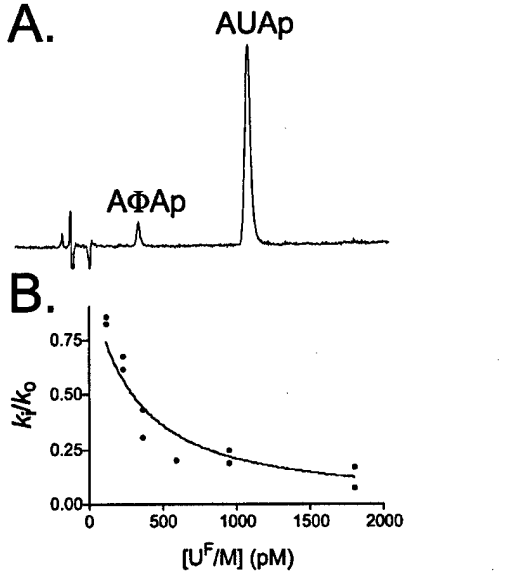

FIGURE 3: Determination of the binding affinity of specific DNA duplexes using a competitive inhibition assay. (A) UDG HPLC activity assay. The substrate (AUAp) and product AΦAp are indicated. (B) Inhibition of UDG by a U·M duplex (K_D = 0.24 ± 0.03 nM).

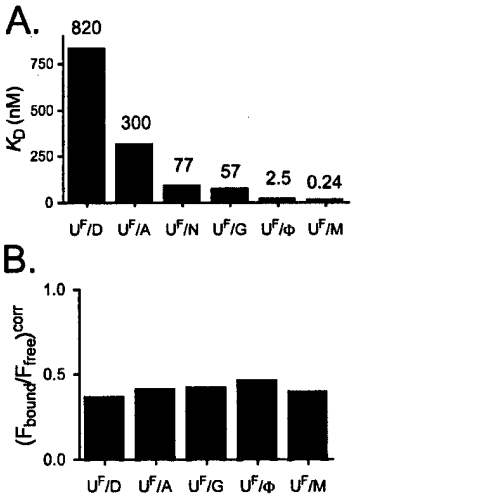

FIGURE 4: (A) Binding affinities of UDG for $U^F \cdot X_n$ DNA duplexes. The K_D values (nanomolar) are shown above the individual bars. (B) Quench of UDG tryptophan fluorescence upon binding of the $U^F \cdot X_n$ duplex. The degree of UDG quenching was normalized to reflect the quenching when UDG is saturated with DNA (see Experimental Procedures).

the six duplexes showed an incremental decrease as the number of hydrogen bonds was ablated (Figure 4A). The tightest observed binding affinity was for the $U^F \cdot M$ construct that has no hydrogen bonds (K_D = 0.25 nM). This affinity is 3000-fold tighter than that of the uracil·diaminopurine duplex that has three hydrogen bonds ($U^F \cdot D$, K_D = 820 nM). Similar tight binding was observed for the duplex with an abasic site opposite U^F ($U^F \cdot \Phi$, K_D = 2.4 nM), providing additional evidence that complete ablation of hydrogen bonding leads to a significantly increased binding affinity.[3]

[3] The observed K_D for the $U^F \cdot \Phi$ duplex (2.5 nM) predominantly reflects binding of UDG to U^F, and not to Φ, because the K_D for abasic DNA is much weaker (70 nM for T·Φ and 100 nM for Φ·A).

Table 1: Thermodynamic Parameters for UDG Binding, DNA Melting, and Permanganate Accessibility of Destabilized Base Pairs

duplex	K_D (nM)	ΔG_{bind} (kcal/mol)	ΔH_{melt} (kcal/mol)	ΔS_{melt} (cal mol^{-1} K^{-1})	ΔG_{melt}[a] (kcal/mol)	log S[b]
U^F·D	820 ± 90	−8.3 ± 0.1	58.9 ± 1.8	0.16 ± 0.01	10.9 ± 2.3	−1.4 ± 0.14
U^F·A	300 ± 50	−8.9 ± 0.1	39.6 ± 4.0	0.11 ± 0.01	7.1 ± 5.2	−1.0 ± 0.06
U^F·N	77 ± 11	−9.7 ± 0.1	40.5 ± 2.0	0.10 ± 0.01	9.2 ± 2.5	ND[c]
U^F·G	57 ± 6	−9.9 ± 0.1	34.0 ± 2.4	0.10 ± 0.01	5.6 ± 3.2	−0.80 ± 0.03
U^F·Φ[3]	2.5 ± 0.4	−11.7 ± 0.1	4.3 ± 0.1	0.01 ± 0.01	0.3 ± 0.3	−0.22 ± 0.01
U^F·M	0.24 ± 0.03	−13.1 ± 0.1	ND[c]	ND[c]	ND[c]	−0.36 ± 0.01

[a] Calculated at 298 K. [b] S is the relative sensitivity of a T·X base pair to oxidation by $KMnO_4$ (see the legend of Figure 6). [c] Not determined.

These results indicate that removal of three hydrogen bonds can enhance specific recognition by up to 4.8 kcal/mol.

In large part, these binding effects reflect the thermodynamic properties of the free damaged site because these discrete base pair perturbations are not expected to affect interactions between UDG and the DNA.[4] This conclusion is supported by inspection of the crystal structures of UDG complexed with substrate analogues, which show that UDG does not make any interactions with the base that opposes the damage site, or with the undamaged strand (*36*). Thus, recognition solely involves the extrahelical deoxyuridine and not other specific features of the base pair or duplex. To further establish that all of the U^F·X duplexes used here attain the same bound state, and that the observed effects on binding largely arise from the properties of the free DNA, we measured the tryptophan fluorescence quenching upon binding of each duplex (Figure 4B). Previous work has shown that the quenching of UDG tryptophan fluorescence upon specific DNA binding is a sensitive measure of an induced fit conformational change in UDG that is required to achieve the final productive conformation with a flipped-out uracil (*5*). Within the errors of these measurements, all of the duplexes produced the same magnitude of fluorescence quenching, indicating that the same bound conformations were attained for all.

Thermodynamic Stabilities of U^F·X Duplexes. We then determined the energetic effects of this series of site-specific base pair disruptions on the thermodynamic parameters for DNA melting using differential scanning calorimetry (DSC, Figure 5). With DSC, one can measure the enthalpy (ΔH_{melt}) and entropy (ΔS_{melt}) of the melting transition directly, and unlike optical methods, it is insensitive to the mechanism of duplex melting (*37*). The free energy of duplex dissociation (ΔG_{melt}) at any temperature can then be simply calculated from ΔH_{melt} and ΔS_{melt}, using the relationship $\Delta G_{melt} = \Delta H_{melt} - T\Delta S_{melt}$, because the heat capacity of the duplex and that of the single strands are equal ($\Delta C_p \approx 0$) (*38*, *39*). As expected, U^F·X duplexes exhibited decreasing transition enthalpies in the ΔH_{melt} range of 58.9−4.3 kcal/mol as the number of hydrogen bonds was decreased. The complete thermodynamic parameters for duplex melting are reported in Table 1.

Correlation of UDG Binding Affinity with Damaged Base Pair Stability. To quantitatively evaluate the impact of damaged base pair disruption on UDG affinity, the differences in binding free energies ($\Delta\Delta G_{bind}$, Figure 1) were plotted against the changes in transition enthalpies ($\Delta\Delta H_{melt}$) and entropies ($-T\Delta\Delta S_{melt}$) (Figure 6A,B). In this analysis, the difference energies are relative to the duplex with three hydrogen bonds (U^F·D), and the value of $-T\Delta\Delta S_{melt}$ was calculated at 298 K. $\Delta\Delta G_{bind}$ was found to increase linearly as the transition enthalpy and entropy decrease: $\Delta\Delta H_{melt}$ (slope = 0.064 ± 0.01, r^2 = 0.937) and $-T\Delta\Delta S_{melt}$ (slope = 0.080 ± 0.011, r^2 = 0.949). As required from these linear correlations, a strong correlation with $\Delta\Delta G_{melt}$ (slope = 0.3 ± 0.1, r^2 = 0.839) was also observed (data not shown). The implications of these correlations are discussed below.

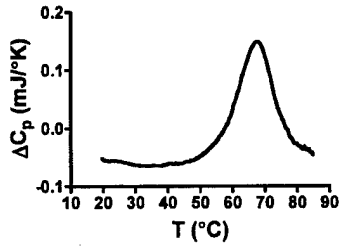

FIGURE 5: Differential scanning calorimetry (DSC) of the U^F·D duplex. A 20 μM DNA duplex solution in 10 mM sodium phosphate (pH 7.5) and 60 mM NaCl was placed inside of the DSC sample cell, and the change in the heat capacity of the solution (ΔC_p) was monitored as it was warmed from 20 to 95 °C at a rate of 60 °C/h. The thermodynamic parameters of duplex dissociation were extracted as described in Experimental Procedures.

Correlation of UDG Binding Affinity with Damaged Base Accessibility. The above thermodynamic correlations suggest that these destabilized duplexes might exhibit an increase in the number of dynamic fluctuations that promote extrahelical states of U^F at temperatures well below the duplex melting temperature. Since the dynamic accessibility of the damaged base is another factor that could enhance its recognition by DNA glycosylases, it was of interest to measure the relative accessibility of each destabilized base pair, and correlate this parameter with UDG binding affinity.

To explore this question, a potassium permanganate ($KMnO_4$) sensitivity assay was employed (*32*, *35*, *40*). Since sites of pyrimidine oxidation are susceptible to strand cleavage under basic conditions, they can be detected as fragments using polyacrylamide gel electrophoresis (Figure 7A) (*41*). In these studies, U^F was first replaced with thymine (T) because of its poor oxidation reactivity arising from its electron deficient 5,6-double bond (data not shown). This is a very conservative change, as a T·X base pair will have base pairing strength and geometry nearly identical to those of a U^F·X base pair (*42*, *43*). As shown in Figure 7A, decreasing the base pair strength leads to an increase in the sensitivity of the T·X base pair to permanganate oxidation, and also the invariant T·A base pair three nucleotides away,

[4] The observation of linear free energy relationships between the thermodynamic parameters of the free duplex DNA and the overall free energy of DNA binding is not negated if different energetic interactions exist between the enzyme and each bound duplex. However, the observed slopes will reflect the relative effects of perturbing the duplex in the free and bound state.

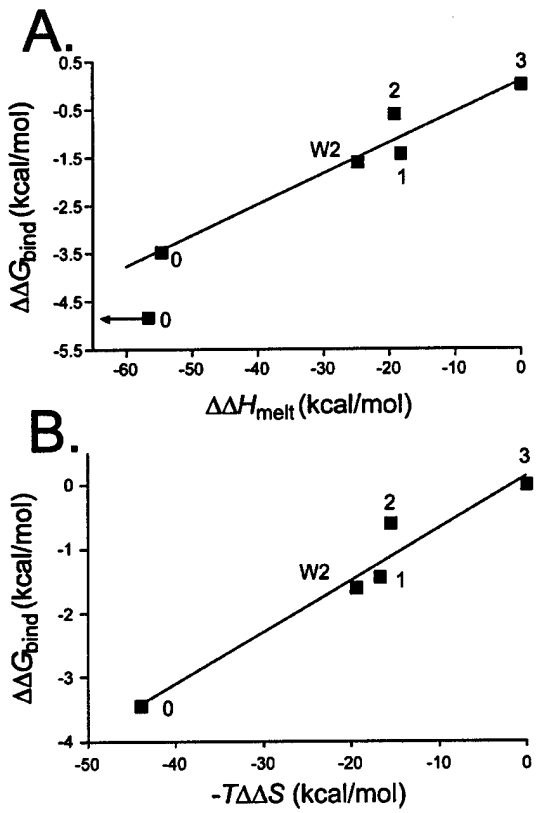

FIGURE 6: Correlations between UDG binding affinity for each $U^F \cdot X_n$ duplex ($\Delta\Delta G_{bind}$) and the thermodynamic parameters for duplex melting. The numbers of hydrogen bonds in the $U^F \cdot X_n$ base pair are indicated. (A) $\Delta\Delta G_{bind}$ vs $\Delta\Delta H_{melt}$ (slope = 0.064, r^2 = 0.937). Only an upper limit for the enthalpy of melting for the $U^F \cdot M$ duplex was obtained (arrow). (B) $\Delta\Delta G_{bind}$ vs $-T\Delta\Delta S_{melt}$ (slope = 0.080, r^2 = 0.949).

indicating that even very conservative changes to the T·X base pair can influence the dynamics of neighboring base pairs in the duplex (*44*). A plot of log K_D against log(relative $KMnO_4$ sensitivity) shows a linear correlation (Figure 7B), establishing that increasing base accessibility at temperatures well below the T_m value has a strong positive effect on binding affinity. As an important control, the amount of oxidized product was found to increase linearly with respect to time and concentration of $KMnO_4$ (data not shown). Therefore, the differences in the sensitivity of these duplexes to oxidation directly reflect the unfavorable dynamic pre-equilibrium for exposure of the thymidine base prior to reaction with $KMnO_4$.

DISCUSSION

Thermodynamic Framework for Active and Passive Base Flipping. While it is clear from structural and spectroscopic studies that DNA glycosylases bind their cognate damaged base in an extrahelical conformation (*3*, *11*), the pathway by which the damaged base is flipped out of the DNA duplex and placed inside of the enzyme active site remains poorly defined. In one model, DNA glycosylases *passively* capture damaged bases that are transiently extrahelical (Figure 8) (*14*, *45*). According to this view, the DNA glycosylase does not lower the activation energy or equilibrium for damaged base flipping, but instead relies on the increased extrahelical propensity of damaged bases to enhance bimolecular encounter. In the alternative view, DNA glycosylases *actively* flip out their cognate lesions by destabilizing the damaged site in an initial encounter complex. Active base flipping may occur by stabilization of high-energy intermediate conformations on the base flipping pathway, or by the use of mechanical forces to propel the base from the duplex (Figure 8) (*5*, *46*). It is important to point out that passive and active flipping pathways cannot be distinguished by *thermodynamic measurements alone.* This conclusion is required because $K_{in}^{bind} K^{enz}_{flip} = K^{non}_{flip} K_{out}^{bind}$, as shown in

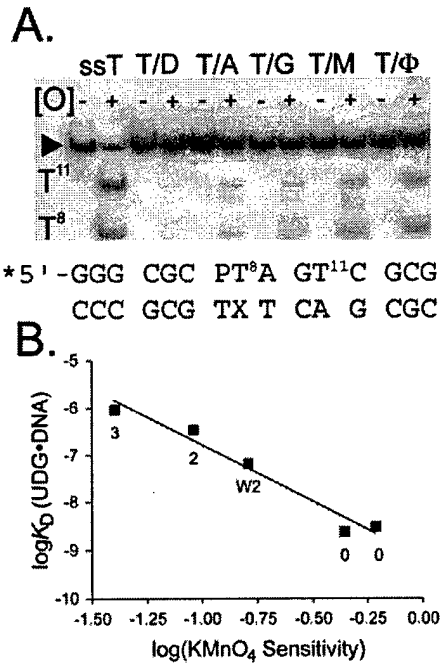

FIGURE 7: (A) Sensitivity of thymine in single-stranded and duplex DNA to oxidation by potassium permanganate. Samples of 5′-^{32}P-labeled single-stranded or $T \cdot X_n$ duplex DNAs were reacted with 2.5 mM $KMnO_4$ ([O]) for 3 min. After the oxidized strands had been cleaved with piperidine, the reaction mixtures were run a 19% denaturing polyacrylamide gel, and the radioactivity of each band was quantified with a phosphorimager. The position on the gel of the full-length DNA is marked with a black wedge. (B) Correlation between UDG binding affinity and $KMnO_4$ sensitivity (slope = -2.37 ± 0.270, r^2 = 0.963). The relative sensitivity of a thymine in a $T \cdot X_n$ base pair is defined as $[(I^{T8} - I^{bkgd})/(I^{total} - I^{bkgd})^{duplex} \times 100]/[(I^{T8} - I^{bkgd})/(I^{total} - I^{bkgd})^{single-stranded} \times 100]$, where I^{T8} is the intensity of the band corresponding to oxidation of the T in the $T \cdot X_n$ base pair, I^{bkgd} is the background correction, and I^{total} is the sum of all of the intensities of the bands in a given lane. The numbers of hydrogen bonds in the $T \cdot X_n$ duplex are indicated.

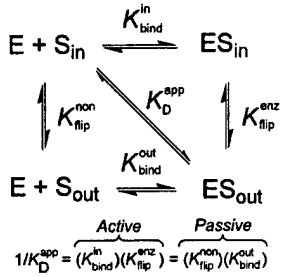

FIGURE 8: Thermodynamic model showing the energetic equivalence of the passive and active base flipping mechanisms (see the text). The equivalence of the pathways is illustrated by the thermodynamic box, which requires that $1/K_D^{app} = K_{in}^{bind} K^{enz}_{flip} = K^{non}_{flip} K_{out}^{bind}$.

Figure 8. Only an assessment of the *kinetic competence* of each pathway can reveal whether passive or active base flipping is the major route taken for a given system.

Specific Recognition and Conformational Freedom of Damaged Sites. We have found that the affinity of UDG for a specific site is linearly dependent on the enthalpy of duplex dissociation (Figure 6A). The linear relationship between UDG affinity and ΔH_{melt} confirms the notion that weakened base pairing decreases the enthalpy of duplex melting and, consequently, increases UDG binding affinity (Figure 6A). However, this finding alone provides little insight into the physical mechanism by which decreases in base pair enthalpy lead to enhanced binding. The small slope of the correlation suggests that the higher affinity of UDG for destabilized damaged sites does not simply arise from the reduced enthalpic cost of breaking a destabilized base pair during base flipping, and that other energetic influences must be at work.[4] It should be stated that the experiments presented here are explicitly designed to probe the enthalpic and entropic contributions of the damaged site alone to specific recognition. The total enthalpy and entropy of binding (including the enzyme, DNA, and solvent) are not evaluated in any of the current experiments, and in fact, these measurements are not required for the conclusions presented below.

The plot of $\Delta\Delta G_{bind}$ versus $-T\Delta\Delta S_{melt}$ reveals that there is an equally significant correlation between changes in duplex entropy and binding affinity (Figure 6B). The parameter $-T\Delta\Delta S_{melt}$ likely reflects the increased conformational flexibility of the destabilized base pairs in the duplex DNA, because the entropy differences of the dissociated single-stranded DNAs in the melting experiments should be similar, given the conservative changes in these substrates. If we assume this physical interpretation for the entropy changes between these DNA constructs, the correlation suggests that increased flexibility of the base pair produces conformational states that are productive for UDG binding. The conclusion that extrahelical conformational states are produced is supported by the correlation between UDG binding affinity and $KMnO_4$ sensitivity (Figure 7B), which reflects the dynamic equilibrium of the base between an inaccessible and permanganate accessible state (i.e., an extrahelical exposed conformation). A reasonable interpretation of these combined findings is that enthalpic destabilization of the base pair allows increased conformational flexibility, producing extrahelical conformers, some of which favor enzyme binding.

The effects of base pair enthalpy and entropy on the extrahelical conformational distributions that may promote base flipping are depicted in Figure 9A–C. In these panels, the probability of an extrahelical conformation is plotted against the backbone pseudodihedral angle (ψ) of the deoxyuridine nucleotide, defined as indicated in Figure 9. The angle ψ has been previously used in computational studies to describe the pathway for base flipping (*47*), and is used here because of its simple representation of the base flipping trajectory, although none of the arguments depend on this formalism. Using this nomenclature, a ψ of 10° reflects the fully base paired state and a ψ of 180° reflects the fully extrahelical state. In free DNA (Figure 9A), the U nucleotide in the stable base pair with three hydrogen bonds (U·D) should be tightly centered around an average conformation with a ψ of 10° (red curve), while the unstable

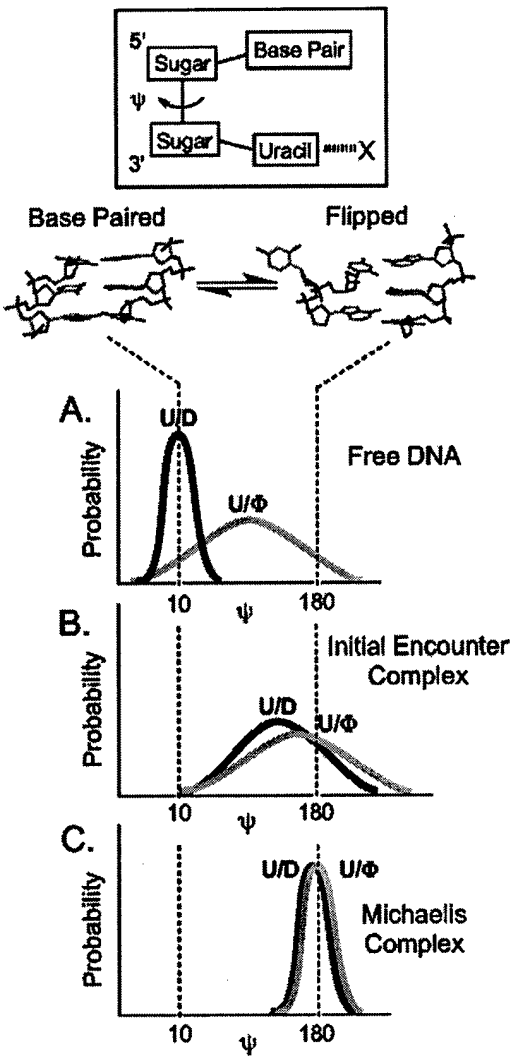

FIGURE 9: Enthalpic destabilization of the U·X$_n$ base pair leads to extrahelical conformations that promote binding. The probability of an extrahelical conformer as a function of the pseudodihedral angle ψ, which is a measure of the progress along the base flipping reaction coordinate, is indicated (see the text and ref *47*). Using this nomenclature, a fully stacked base pair has a ψ value of ~10°, whereas the fully extrahelical conformation has a ψ value of 180°. (A) Enthalpic destabilization of the base pair in the free DNA leads to extrahelical conformations that promote *passive* base flipping. (B) Base pair destabilization can also affect an active mechanism in which UDG forms an initial encounter complex with the DNA in which the base is not yet fully extrahelical (*5*, *46*, *48*). In this case, enzyme binding energy is used to destabilize the U·D base pair, allowing it to achieve extrahelical states already available to the U·Φ duplex due to its intrinsic instability. (C) A hypothetical distribution of extrahelical conformers for the final UDG·DNA complex. The enzyme has fully stabilized the flipped-out uracil, and the distribution of conformational states for the U·D and U·Φ duplexes is narrowly focused around a ψ of 180° (*36*, *47*).

construct with no hydrogen bonds (U·Φ) should be broadly centered around a ψ value further along the flipping reaction coordinate (green curve). Thus, enthalpic destabilization of the base pair in a passive mechanism leads to conformations that facilitate binding of the enzyme (see Figure 8, counterclockwise pathway).

For the alternative active base flipping mechanism (Figure 9B), binding of UDG in an initial encounter complex can

alter the DNA structure such that the more stable U·D base pair is also destabilized (Figure 9B, red curve) (*5*, *46*, *48*). In this initial destabilized complex, the partially extrahelical uracil may assume a similar average conformation, and broad distribution, for both the U·D and U·Φ constructs. However, flipping of U in the U·D construct requires a greater amount of binding energy to overcome the enthalpic barrier to base flipping, resulting in weaker binding of the U·D duplex compared to that of the U·Φ duplex. Finally, in the Michaelis complex, in which the base is fully extrahelical (Figure 9C), both the U·D and U·Φ duplexes assume the same average conformation and small conformational distribution which are enforced by the strong interactions between the enzyme and uracil (*36*, *46*). Although this mechanism implies a reduction in the conformational flexibility of destabilized base pairs such as the U·Φ duplex upon formation of the Michaelis complex, this expected unfavorable entropic contribution to the overall free energy of binding may be paid for by the even larger enthalpic benefit of base pair destabilization for such conformationally flexible substrates (Table 1).

CONCLUSIONS

We have shown that the maximum gain in specific recognition by UDG arising from destabilization of the damaged base pair is 4.8 kcal/mol, and that this energetic effect likely arises from increasing the population of extrahelical states that promote binding. Since the catalytic specificity of UDG for uracil as opposed to other normal bases has been estimated to be at least 8.3 kcal/mol *in vitro* (*5*), the energetic contribution of destabilized damaged sites to specific ground state binding can be significant, at least in this model system. However, the *in vivo* substrates of UDG consist of U·A or U·G base pairs, which are not significantly destabilized compared to other normal base pairs. Thus, spontaneous base flipping at damaged sites is not a viable mechanism for accounting for the specificity of UDG *in vivo*. The remaining specificity of UDG must be attributed to strong transition state interactions that can be induced only by actively flipping the uracil base into the active site (*5*, *49*). Although unimportant for UDG, damaged site instability could contribute significantly to specific recognition by repair enzymes that act on intrinsically unstable base pairs such as O^6-methylguanine (*45*), hypoxanthine (*50*, *51*), N^1-methyladenine, and N^3-methylcytosine (*52*, *53*).

ACKNOWLEDGMENT

We thank Prof. Paul Miller at the Johns Hopkins School of Public Health for the generous use of his solid-phase DNA synthesizer.

REFERENCES

1. Lindahl, T. (1993) Instability and decay of the primary structure of DNA, *Nature 362*, 709−715.
2. Seeberg, E., Eide, L., and Bjoras, M. (1995) The base excision repair pathway, *Trends Biochem. Sci. 20*, 391−397.
3. Mol, C. D., Parikh, S. S., Putnam, C. D., Lo, T. P., and Tainer, J. A. (1999) DNA repair mechanisms for the recognition and removal of damaged DNA bases, *Annu. Rev. Biophys. Biomol. Struct. 28*, 101−128.
4. Stivers, J. T., and Jiang, Y. L. (2003) A mechanistic perspective on the chemistry of DNA repair glycosylases, *Chem. Rev. 103*, 2729−2759.
5. Stivers, J. T., Pankiewicz, K. W., and Watanabe, K. A. (1999) Kinetic mechanism of damage site recognition and uracil flipping by *Escherichia coli* uracil DNA glycosylase, *Biochemistry 38*, 952−963.
6. Lindahl, T., and Andersson, A. (1972) Rate of chain breakage at apurinic sites in double-stranded deoxyribonucleic acid, *Biochemistry 11*, 3618−3623.
7. Cuniasse, P., Fazakerley, G. V., Guschlbauer, W., Kaplan, B. E., and Sowers, L. C. (1990) The abasic site as a challenge to DNA polymerase. A nuclear magnetic resonance study of G, C and T opposite a model abasic site, *J. Mol. Biol. 213*, 303−314.
8. Lindahl, T. (1990) Repair of intrinsic DNA lesions, *Mutat. Res. 238*, 305−311.
9. Kavli, B., Slupphaug, G., Mol, C. D., Arvai, A. S., Peterson, S. B., Tainer, J. A., and Krokan, H. E. (1996) Excision of cytosine and thymine from DNA by mutants of human uracil-DNA glycosylase, *EMBO J. 15*, 3442−3447.
10. Kwon, K., Jiang, Y., and Stivers, J. (2003) Rational Engineering of a DNA Glycosylase Specific for Unnatural Cytosine:Pyrene Base Pairs, *Chem. Biol. 10*, 1−9.
11. Slupphaug, G., Mol, C. D., Kavli, B., Arvai, A. S., Krokan, H. E., and Tainer, J. A. (1996) A nucleotide-flipping mechanism from the structure of human uracil-DNA glycosylase bound to DNA, *Nature 384*, 87−92.
12. Klimasauskas, S., Kumar, S., Roberts, R. J., and Cheng, X. (1994) HhaI methyltransferase flips its target base out of the DNA helix, *Cell 76*, 357−369.
13. Verdine, G. L., and Bruner, S. D. (1997) How do DNA repair proteins locate damaged bases in the genome? *Chem. Biol. 4*, 329−334.
14. Pearl, L. H. (2000) Structure and function in the uracil-DNA glycosylase superfamily, *Mutat. Res. 460*, 165−181.
15. Vallur, A. C., Feller, J. A., Abner, C. W., Tran, R. K., and Bloom, L. B. (2002) Effects of hydrogen bonding within a damaged base pair on the activity of wild type and DNA-intercalating mutants of human alkyladenine DNA glycosylase, *J. Biol. Chem. 277*, 31673−31678.
16. Osman, R., Fuxreiter, M., and Luo, N. (2000) Specificity of damage recognition and catalysis of DNA repair, *Comput. Chem. 24*, 331−339.
17. Fuxreiter, M., Luo, N., Jedlovszky, P., Simon, I., and Osman, R. (2002) Role of base flipping in specific recognition of damaged DNA by repair enzymes, *J. Mol. Biol. 323*, 823−834.
18. Liu, P., Burdzy, A., and Sowers, L. C. (2002) Substrate recognition by a family of uracil-DNA glycosylases: UNG, MUG, and TDG, *Chem. Res. Toxicol. 15*, 1001−1009.
19. Valinluck, V., Liu, P., Burdzy, A., Ryu, J., and Sowers, L. C. (2002) Influence of Local Duplex Stability and N(6)-Methyladenine on Uracil Recognition by Mismatch-Specific Uracil-DNA Glycosylase (Mug), *Chem. Res. Toxicol. 15*, 1595−1601.
20. Biswas, T., Clos, L. J., II, SantaLucia, J., Jr., Mitra, S., and Roy, R. (2002) Binding of specific DNA base-pair mismatches by *N*-methylpurine-DNA glycosylase and its implication in initial damage recognition, *J. Mol. Biol. 320*, 503−513.
21. Panayotou, G., Brown, T., Barlow, T., Pearl, L. H., and Savva, R. (1998) Direct measurement of the substrate preference of uracil-DNA glycosylase, *J. Biol. Chem. 273*, 45−50.
22. Chepanoske, C. L., Langelier, C. R., Chmiel, N. H., and David, S. S. (2000) Recognition of the nonpolar base 4-methylindole in DNA by the DNA repair adenine glycosylase MutY, *Org. Lett. 2*, 1341−1344.
23. Fromme, J. C., and Verdine, G. L. (2002) Structural insights into lesion recognition and repair by the bacterial 8-oxoguanine DNA glycosylase MutM, *Nat. Struct. Biol. 9*, 544−552.
24. Bernards, A. S., Miller, J. K., Bao, K. K., and Wong, I. (2002) Flipping duplex DNA inside-out: A double base-flipping reaction mechanism by *Escherichia coli* MutY adenine glycosylase, *J. Biol. Chem. 277*, 20960−20964.
25. Barrett, T. E., Savva, R., Panayotou, G., Barlow, T., Brown, T., Jiricny, J., and Pearl, L. H. (1998) Crystal structure of a G:T/U mismatch-specific DNA glycosylase: mismatch recognition by complementary-strand interactions, *Cell 92*, 117−129.
26. Lindahl, T. (1974) An N-glycosidase from *Escherichia coli* that releases free uracil from DNA containing deaminated cytosine residues, *Proc. Natl. Acad. Sci. U.S.A. 71*, 3649−3653.

27. Stivers, J. T., and Drohat, A. C. (2001) Uracil DNA glycosylase: insights from a master catalyst, *Arch. Biochem. Biophys. 396*, 1−9.
28. Watanabe, K. A., Reichman, U., Hirota, K., Lopez, C., and Fox, J. J. (1979) Nucleosides. 110. Synthesis and antiherpes virus activity of some 2′-fluoro-2′-deoxyarabinofuranosylpyrimidine nucleosides, *J. Med. Chem. 22*, 21−24.
29. Fasman, G. D. (1975) *Handbook of Biochemistry and Molecular Biology: Nucleic Acids*, 3rd ed., Vol. 1, CRC Press, Boca Raton, FL.
30. Drohat, A. C., Jagadeesh, J., Ferguson, E., and Stivers, J. T. (1999) The role of electrophilic and base catalysis in the mechanism of *Escherichia coli* uracil DNA glycosylase, *Biochemistry 38*, 11866−11875.
31. Jiang, Y. L., and Stivers, J. T. (2001) Reconstructing the substrate for uracil DNA glycosylase: tracking the transmission of binding energy in catalysis, *Biochemistry 40*, 7710−7719.
32. Jiang, Y. L., Kwon, K., and Stivers, J. T. (2001) Turning on uracil-DNA glycosylase using a pyrene nucleotide switch, *J. Biol. Chem. 276*, 42347−42354.
33. Chakrabarti, M. C., and Schwarz, F. P. (1999) Thermal stability of PNA/DNA and DNA/DNA duplexes by differential scanning calorimetry, *Nucleic Acids Res. 27*, 4801−4806.
34. Kirchoff, W. H. (1993) Exam: A Two-State Thermodynamic Analysis Program, NIST Technical Note 1401, pp 1−103, National Institute of Standards and Technology.
35. Jones, A. S., and Walker, R. T. (1963) The permanganate oxidation of nucleosides, *J. Chem. Soc.*, 3554−3557.
36. Parikh, S. S., Walcher, G., Jones, G. D., Slupphaug, G., Krokan, H. E., Blackburn, G. M., and Tainer, J. A. (2000) Uracil-DNA glycosylase-DNA substrate and product structures: conformational strain promotes catalytic efficiency by coupled stereoelectronic effects, *Proc. Natl. Acad. Sci. U.S.A. 97*, 5083−5088.
37. Breslauer, K. J. (1995) Extracting thermodynamic data from equilibrium melting curves for oligonucleotide order−disorder transitions, *Methods Enzymol. 259*, 221−242.
38. Plum, G. E., Grollman, A. P., Johnson, F., and Breslauer, K. J. (1995) Influence of the oxidatively damaged adduct 8-oxodeoxyguanosine on the conformation, energetics, and thermodynamic stability of a DNA duplex, *Biochemistry 34*, 16148−16160.
39. Breslauer, K. J., Frank, R., Blocker, H., and Marky, L. A. (1986) Predicting DNA duplex stability from the base sequence, *Proc. Natl. Acad. Sci. U.S.A. 83*, 3746−3750.
40. Hayatsu, H., and Ukita, T. (1967) The selective degradation of pyrmidines in nucleic acids by permanganate oxidation, *Biochem. Biophys. Res. Commun. 29*, 556−561.
41. Rubin, C. M., and Schmid, C. W. (1980) Pyrimidine-specfic chemical reactions useful for DNA sequencing, *Nucleic Acids Res. 8*, 4613−4619.
42. Delort, A. M., Neumann, J. M., Molko, D., Herve, M., Teoule, R., and Tran Dinh, S. (1985) Influence of uracil defect on DNA structure: ^{1}H NMR investigation at 500 MHz, *Nucleic Acids Res. 13*, 3343−3355.
43. Saenger, W. (1984) *Principles of Nucleic Acid Structure*, Springer-Verlag, New York.
44. Moe, J. G., and Russu, I. M. (1992) Kinetics and energetics of base-pair opening in 5′-d(CGCGAATTCGCG)-3′ and a substituted dodecamer containing G·T mismatches, *Biochemistry 31*, 8421−8428.
45. Duguid, E. M., Mishina, Y., and He, C. (2003) How Do DNA Repair Proteins Locate Potential Base Lesions? A Chemical Crosslinking Method to Investigate O(6)-Alkylguanine-DNA Alkyltransferases, *Chem. Biol. 10*, 827−835.
46. Huang, N., Banavali, N. K., and MacKerell, A. D., Jr. (2003) Protein-facilitated base flipping in DNA by cytosine-5-methyltransferase, *Proc. Natl. Acad. Sci. U.S.A. 100*, 68−73.
47. Banavali, N. K., and MacKerell, A. D., Jr. (2002) Free energy and structural pathways of base flipping in a DNA GCGC containing sequence, *J. Mol. Biol. 319*, 141−160.
48. Jiang, Y. L., and Stivers, J. T. (2002) Mutational analysis of the base flipping mechanism of uracil DNA glycosylase, *Biochemistry 41*, 11236−11247.
49. Jiang, Y. L., Drohat, A. C., Ichikawa, Y., and Stivers, J. T. (2002) Probing the Limits of Electrostatic Catalysis by Uracil DNA Glycosylase Using Transition-State Mimicry and Mutagenesis, *J. Biol. Chem. 277*, 15385−15392.
50. Case-Green, S. C., and Southern, E. M. (1994) Studies on the base pairing properties of deoxyinosine by solid phase hybridisation to oligonucleotides, *Nucleic Acids Res. 22*, 131−136.
51. Wyatt, M. D., and Samson, L. D. (2000) Influence of DNA structure on hypoxanthine and 1,N(6)-ethenoadenine removal by murine 3-methyladenine DNA glycosylase, *Carcinogenesis 21*, 901−908.
52. Trewick, S. C., Henshaw, T. F., Hausinger, R. P., Lindahl, T., and Sedgwick, B. (2002) Oxidative demethylation by *Escherichia coli* AlkB directly reverts DNA base damage, *Nature 419*, 174−178.
53. Falnes, P. O., Johansen, R. F., and Seeberg, E. (2002) AlkB-mediated oxidative demethylation reverses DNA damage in *Escherichia coli*, *Nature 419*, 178−182.
54. Cheong, C., Tinoco, I., Jr., and Chollet, A. (1988) Thermodynamic studies of base pairing involving 2,6-diaminopurine, *Nucleic Acids Res. 16*, 5115−5122.
55. Howard, F. B., Frazier, J., and Miles, H. T. (1966) A new polynucleotide complex stabilized by 3 interbase hydrogen bonds, poly-2-aminoadenylic acid + polyuridylic acid, *J. Biol. Chem. 241*, 4293−4295.
56. Carbonnaux, C., Fazakerley, G. V., and Sowers, L. C. (1990) An NMR structural study of deaminated base pairs in DNA, *Nucleic Acids Res. 18*, 4075−4081.
57. Ikuta, S., Eritja, R., Kaplan, B. E., and Itakura, K. (1987) NMR studies of the stable mismatch purine-thymine in the self-complementary d(CGPuAATTTCG) duplex in solution, *Biochemistry 26*, 5646−5650.
58. Clore, G. M., Oschkinat, H., McLaughlin, L. W., Benseler, F., Happ, C. S., Happ, E., and Gronenborn, A. M. (1988) Refinement of the solution structure of the DNA dodecamer 5′d(CGCGPATTCGCG)$_2$ containing a stable purine-thymine base pair: combined use of nuclear magnetic resonance and restrained molecular dynamics, *Biochemistry 27*, 4185−4197.
59. Cuniasse, P., Sowers, L. C., Eritja, R., Kaplan, B., Goodman, M. F., Cognet, J. A., LeBret, M., Guschlbauer, W., and Fazakerley, G. V. (1987) An abasic site in DNA. Solution conformation determined by proton NMR and molecular mechanics calculations, *Nucleic Acids Res. 15*, 8003−8022.
60. Goljer, I., Kumar, S., and Bolton, P. H. (1995) Refined solution structure of a DNA heteroduplex containing an aldehydic abasic site, *J. Biol. Chem. 270*, 22980−22987.
61. Coppel, Y., Berthet, N., Coulombeau, C., Coulombeau, C., Garcia, J., and Lhomme, J. (1997) Solution conformation of an abasic DNA undecamer duplex d(CGCACXCACGC) × d(GCGTGTGTGCG): the unpaired thymine stacks inside the helix, *Biochemistry 36*, 4817−4830.
62. Moran, S., Ren, R. X., Sheils, C. J., Rumney, S. t., and Kool, E. T. (1996) Non-hydrogen bonding "terminator" nucleosides increase the 3′-end homogeneity of enzymatic RNA and DNA synthesis, *Nucleic Acids Res. 24*, 2044−2052.

BI036303Y